Research Article

Veysel Özlü and Müge Elif Fırat*

Fly ash and nano-graphene enhanced stabilization of engine oil-contaminated soils

https://doi.org/10.1515/ntrev-2025-0210
received June 3, 2025; accepted August 17, 2025

Abstract: Due to urbanization and population growth, the redevelopment of contaminated areas has become popular. Engine oil, used for lubricating various engines, absorbs additional components from wear. Although used oils can be recycled if collected properly, they are often dumped, leading to groundwater and soil contamination. When incorporated into natural soils, these materials deteriorate environmental quality and adversely impact the geotechnical performance of the soil. This study investigates the impact of waste engine oil (EO)-contaminated kaolin (0, 3, 5, and 9%) on its physical and engineering behavior and evaluates the effectiveness of stabilization using fly ash at 0, 10, 25, and 45%, as well as nano-graphene at 0.04, 0.08, and 0.12%. The influence of contamination duration on these properties was thoroughly examined, and the optimal proportions of mineral additives and nanoparticle materials were identified through Gray Relational Analysis, ensuring enhanced precision in performance optimization. The results show that EO contamination increases the liquid limit due to the reduced water absorption capacity and increases the plastic limit to a greater extent, leading to a decrease in the plasticity index. The addition of fly ash (FA) and nano-graphene affects the physical properties differently based on the contamination levels. The water content of the contaminated kaolin decreased, while the dry unit weight increased. EO contamination reduces the unconfined compressive strength (UCS), and higher contamination degrees result in greater reduction. The inclusion of fly ash (FA) significantly enhances the UCS, with pronounced improvements observed at higher replacement ratios. The peak UCS enhancement occurred with the incorporation of 0.08% nanographene. However, both the degree of contamination and the addition of nanographene contributed to the increased brittleness of the soil matrix. The optimal gradation for maximum UCS was found to be 0.12% nanographene with 25% FA at 5% waste engine oil contamination. For the brittleness index, 10% FA and 0.04% nanographene are recommended for 3% engine oil contamination. The study concludes that the addition of mineral additives and nanoparticle materials can improve the geotechnical properties of contaminated soils, with fly ash and nano-graphene being effective additives.

Keywords: kaolin clay, waste engine oil contamination, nanoparticle, fly ash, soil stabilization

1 Introduction

Urbanization and population growth have increased the interest in redeveloping contaminated areas. Human activities like mining, metal industries, and oil extraction are the main sources of pollution, degrading soil quality [1] and altering geotechnical properties [2]. Soil susceptibility to contaminants depends on factors such as mineral composition, particle size, interparticle bonding, and ion exchange capacity. The contaminants can be retained through chemical adsorption, capillary forces, or by forming liquid pools on the clay and silt lenses. As a result, the properties and behavior of infrastructure soils vary, influenced by changes in pore fluid characteristics and soil interactions [3–5]. Investigating these effects and developing engineering solutions for contaminated sites provides both economic advantages and sustainable outcomes for infrastructure development.

Due to the rapid developments in the petroleum and automotive industries, environmental pollution has become a significant concern. Petroleum and its products, such as gasoline, diesel, motor oil, and kerosene, are extensively used in transportation and industry. Motor oil, used for lubrication in various engines, accumulates additional components (lead, chromium, naphthalene, chlorinated hydrocarbons, and sulfur) from engine wear. As the oil viscosity changes over time, proper disposal of used oils is essential. Unfortunately, they are often improperly

* **Corresponding author: Müge Elif Fırat,** Technology Faculty, Civil Engineering Department, Firat University, Elazig, Turkey, e-mail: morakoglu@firat.edu.tr, tel: +90 (424) 607 4283
Veysel Özlü: Technology Faculty, Civil Engineering Department, Firat University, Elazig, Turkey, e-mail: veyselozlu98@gmail.com
ORCID: Veysel Özlü 0000-0003-0330-3923; Müge Elif Fırat 0000-0002-5391-5859

discarded, contaminating the soil and groundwater. When mixed with natural soils, they negatively impact engineering properties, including mechanical and filtration parameters, plasticity, and swelling [2,6,7]. Moreover, oil-contaminated soils exhibit reduced shear strength, increased compressibility, and significant settlement issues under load, which compromise the stability and longevity of foundations and pavements. Contaminants can weaken interparticle bonds, alter the soil's water retention and permeability characteristics, and cause differential settlements or bearing capacity failures. These behaviors not only degrade geotechnical performance but also increase the risk of structural distress in infrastructure systems [8]. This discharge leads to hydrocarbon contamination, polluting the air, soil, and groundwater with toxic and mutagenic polycyclic aromatic hydrocarbons [9–13]. Contaminated areas pose environmental and health risks and create engineering challenges for establishing infrastructure systems, resulting in financial losses and premature mechanical failures. To address these issues, global studies aim to design more stable infrastructure systems with high bearing capacity.

The redevelopment of contaminated areas during rapid urbanization also involves the use of marginal soils with low strength and high deformation characteristics [14,15]. Clay soils, known for their high volume change potential, are frequently used as impermeable elements or protective layers in various engineering structures such as soil embankments, road fills, waste disposal site liners, and nuclear power plants. However, these soils can cause permanent damage to structural elements due to problems such as swelling, shrinkage, settlement, and heaving resulting from changes in water content over time [16–20].

During engineering applications, clay soils used in infrastructure experience changes in water content due to applied loads and environmental factors like climate change. These variations affect the liquid limit of clay soils, which have a high volume change potential. The strength of clays with different plasticity characteristics depends on their structural properties and consistency limits [21–24]. When these soils are contaminated, their geotechnical properties change due to physicochemical interactions with the contaminant [25,26]. Chemical interactions dominate for highly plastic clay soils. The dielectric constant plays a vital role in changing the thickness of the diffuse double layer, with lower values favoring clay flocculation [12,27].

Singh *et al.* [25] studied different soil types, including low-plasticity clay (CL), high-plasticity clay (CH), and poorly graded sand (SP), contaminated with motor oil at various rates. It was observed that volume change properties, including consolidation settlement and swelling behavior, increased with higher levels of contamination in clayey soils (CL and CH). Higher contamination rates led to more settlement and greater sensitivity to volume changes. Liu *et al.* [28] examined kaolin clay contaminated with diesel oil at different ratios. They observed that increased contamination reduced the liquid and plastic limit values, as well as the unconfined compressive strength of the clay.

Studies have shown the harmful effects of petroleum and refinery products on soil, but these studies have been developed independently. Stabilizing clay soils with chemical and mineral additives is a well-researched topic. Mineral additives like cement, lime, fly ash, silica fume, and rice husk ash are commonly used to stabilize problematic soils with large volume change behavior due to seasonal water content variations [29–34]. Some literature studies have examined the use of mineral additives in contaminated areas regarding soil biobeneficiality, environmental quality, and health [35–37]. However, geotechnical property studies in this context are limited.

Recent advances in nanotechnology have led to the extensive use of clay minerals to create nanocomposite materials by modifying their surface chemistry with chemicals and polymers [38–40]. Nanomaterials, with dimensions smaller than 100 nm have unique structures and extremely high specific surface areas and surface activities. Initially used by physicists and chemists, geotechnical engineers and researchers have started utilizing nanomaterials in soil improvement for sustainable and environmentally friendly environments [5,41–43]. Nanotechnology has revolutionized soil stabilization by allowing materials to be designed at the atomic level. Geotechnical engineers have long dealt with nanoscale dimensions and materials, especially concerning the clay structure and water molecules influencing soil plasticity and cohesion. In recent times, nanotechnology and nanomaterials have been used in geotechnical engineering primarily for stabilization and remediation purposes. Excitingly, recent research has demonstrated that using a small amount of nanoparticles (less than 1% of the dry weight of the soil) can lead to significant improvements in the soil properties. This efficient use of materials is crucial for prolonging the lifespan of our depleting natural resources and ensuring sustainability. Among carbon-based nanomaterials, nanographene stands out due to its exceptional surface area, mechanical strength, and chemical stability, which enable it to enhance the interaction with mineral binders like fly ash. While other nanomaterials, such as carbon nanotubes and nano-silica, have been studied, their high cost, lower

dispersibility in soil media, or lesser compatibility with certain binders limit their field application. The synergistic effect of fly ash and nanographene provides both pozzolanic reactivity and nanoscale reinforcement, making them a suitable and sustainable choice for improving oil-contaminated soils [44].

The urgency to address this contamination is particularly evident in rapidly growing urbanization and infrastructure development projects. As oil pollution poses serious threats to both human health and ecosystems, it has become imperative to reclaim polluted areas and develop sustainable infrastructure systems. In this context, the need for effective and sustainable soil remediation solutions to mitigate the negative effects of kaolin from oil pollution remains urgent. This study aims to investigate the physical properties and engineering behaviors of kaolin clays contaminated with different ratios of waste engine oil, along with the impact of the duration of contamination, mineral additives, and nanoparticle materials. It addresses the often overlooked factor of contamination duration on kaolin clay's properties when contaminated with waste engine oil. Additionally, the study explores the use of nanoparticles for soil improvement, an area with potential scientific quality and innovation due to the challenges in finding suitable materials for specialized applications. The study's comprehensive examination of both the geotechnical properties of contaminated soils and the use of nanoparticles for improvement holds significance and innovation potential for geotechnical engineering. The combination of these factors in the study fills a gap in the literature, contributing to the study's originality and unique value.

2 Materials and methods

2.1 Materials

2.1.1 Soil

The kaolin clay used in this study is a type of clay composed of a significant amount of feldspar minerals and layers of silica and aluminum [45]. Kaolin clays constitute a large proportion of the naturally occurring clays in Turkey. Due to their sensitivity to water and resulting reduction in strength, these clays are generally classified as soft clays. Although kaolinite-rich soils are relatively stable and exhibit lower water absorption capacity compared to montmorillonitic or illitic clays, their engineering properties may still degrade upon moisture ingress. Therefore, their behavior under varying moisture conditions, particularly in contaminated environments, requires further investigation [17]. The complex and unpredictable behavior of such soils has led to their recognition as problematic soils in construction projects, and as a result, studies have focused on this type of clay. Over the years, due to urban development and increasing construction trends, land use policies have attempted to build on various soils, including low-strength soils such as kaolin clay.

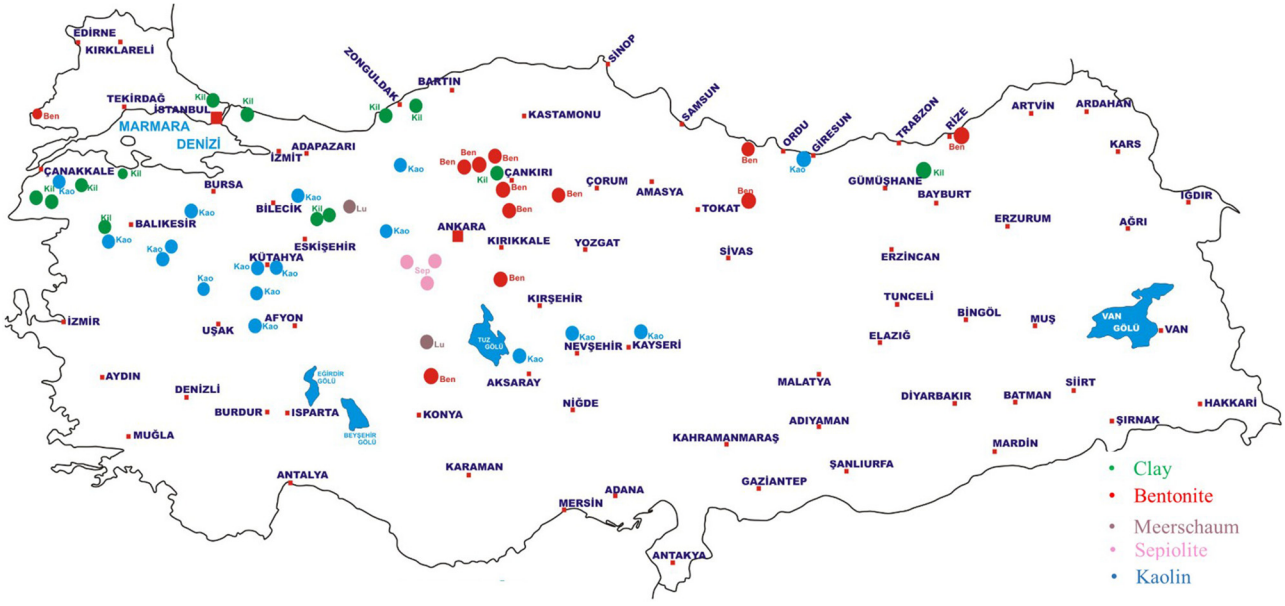

Figure 1: Clay deposits map in Turkey [46].

Table 1: Summary of the properties of kaolin

Properties		Value		ASTM Standard
Grain size* (μm)	D50**	<10 μm	<2 μm	
	1.3	97.1%	60.8%	
Specific gravity	2.65			[47]
Atterberg limits	LL	PL	PI	[48]
	26.15%	17.10%	9.05%	
Compaction parameters	γ_{kmax} 16.5 kN/m^3	w_{opt} 18.32%		[49]

*Grain size distribution based on laser diffraction, **D50 indicates median size.

Table 2: Summary of the chemical properties of kaolin

Chemical Content				Humidity	pH
SiO_2	Al_2O_3	Fe_2O_3	TiO_2	0.37%	6.83
58.40%	37.74%	1.86%	0.63%		

The high occurrence of natural kaolin clays in Turkey and their decreased strength due to the effect of water are among the most important reasons for using kaolin clays in this study. Turkey is among the countries with significant kaolin reserves worldwide (as presented in Figure 1).

The kaolin clay used in the experiments was obtained from Northwest Anatolia, specifically Balikesir province in Turkey. The properties of the clay are presented in Tables 1 and 2.

2.1.2 Waste engine oil

The rapid development of the oil and automotive industries has led to increased environmental pollution, especially from used engine oils. These oils, which contain harmful components such as lead and hydrocarbons, can contaminate the soil if not disposed of properly. Oil contamination negatively affects the soil's mechanical properties, filtration ability, plasticity, and swelling, leading to environmental degradation. Therefore, proper disposal and the development of stable infrastructure systems are essential to prevent further soil and groundwater contamination. In this study, the Helix hx5 diesel 10w-30 engine oil waste obtained from the Elazig industry site, as depicted in Figure 2, was chosen as the contaminant.

Figure 2: Waste engine oil.

The components in the waste engine oil were determined by performing ICP-MS analysis at the Eastern Anatolia High Technology Application and Research Center (DAYTAM) at Atatürk University in Erzurum. The results of the ICP-MS analysis are given in Table 3.

2.1.3 Mineral additive: Fly ash (FA)

Fly ash is commonly used in soil stabilization because of its strength-enhancing properties and cost-effectiveness. Studies on materials such as lime, cement, and fly ash have demonstrated their effectiveness in neutralizing oil contamination in soil. Fly ash, in particular, has proven to be an accessible and economical solution for stabilizing contaminated soils [50–53]. Considering the issues related to soil contamination, this study focuses on the stabilization of kaolin soils contaminated with engine oil using fly ash. As shown in Figure 3, Class-F fly ash, obtained from the Bursa (in Turkey) power plant, was used to stabilize the contaminated kaolin in this study. The chemical compounds of the fly ash are presented in Table 4.

Table 3: The results of the ICP-MS analysis of the waste engine oil

Elements	Al	Cr	Co	Ni	Cu	Zn	As	C	Pb
Concentration (ppm)	13826.144	2320.268	119.664	1301.132	9700.507	949258.24	45.716	19730.723	1902.468

Figure 3: Class-F fly ash.

Table 4: The chemical compounds of the fly ash

	SiO_2	Al_2O_3	Fe_2O_3	CaO	MgO
Class-F fly ash (%)	48.53	24.61	7.59	9.48	2.28

2.1.4 Nanoparticle additive: Nanographene

Graphene, a one-atom-thick layer of carbon atoms, is notable for its high mechanical strength and thermal and electrical conductivity, making it valuable for various engineering applications. Graphene nanopowder, made of nanometer-sized graphene plates, is widely used in numerous fields. The nanographene (NG) used in this study was provided by ALGI LAB and employed for stabilizing the contaminated kaolin. Fly ash was used as a binder because nanographene alone does not possess binding properties.

Figure 4: Nanographene powder used in the study.

The physical properties of the nanographene, as depicted in Figure 4, are presented in Table 5.

2.2 Experimental program

The aim of this study was to assess the impact of fly ash and nanographene on the physical and mechanical properties of kaolin clay contaminated with waste engine oil. The contaminated samples were prepared by introducing varying ratios (0, 3, 5, and 9 wt%) of waste engine oil into the kaolin clay. Stabilization of the contaminated kaolin was achieved by incorporating different ratios (0, 10, 25, and 45%) of fly ash and (0.04, 0.08, and 0.12%) nanographene. Because nanographene lacks inherent binding properties, it was combined with fly ash during the sample preparation. Unconfined compression tests (UCS) were conducted to evaluate the strength characteristics of the contaminated kaolin samples treated with fly ash and nanographene. The experimental program details are provided in Table 6.

In this study, the specific gravity of the mixtures (Gmix) was calculated using the weighted average method, based on the specific gravities and proportions of the individual components. This approach is widely adopted in the literature and has been recommended by Mir and Sridharan [54] for geotechnical applications.

The pure kaolin sample (S1) exhibited the highest specific gravity value of 2.650. The incorporation of EO alone, even at low percentages, resulted in a notable decrease in Gmix. For instance, adding 3, 5, and 9% EO reduced Gmix from 2.650 to 2.515, 2.432, and 2.282, respectively (S2–S4). This trend can be attributed to the relatively low specific gravity of waste engine oil, which, as a light hydrocarbon-based fluid, lowers the overall density of the mix. When FA was introduced alongside EO, a further decline in Gmix was observed. In the EO-fixed mixtures (S5–S10), increasing the FA content from 10 to 45% led to a systematic reduction in Gmix, indicating the cumulative density-reducing effect of fly ash, which itself has a lower specific gravity compared to kaolin. For example, Gmix decreased from 2.475 (S5) to 2.418 (S6) and 2.347 (S7) as the FA content increased from 10 to 45% at constant EO

Table 5: Properties of the NG

	Purity	Size	Surface area	Diameter
NG	99.9%	3 nm	800 m^2/g	1.5 μm

Table 6: The experimental program

No	Sample ID	Material percentage (wt%)				Gmix*	Contamination degree	Tests
		Kaolin	EO	FA	NG			
S1	Pure kaolin	100	0	0	0	2.650	0, 7	UCS
S2	K + 3% EO	97	3	0	0	2.515		Physical tests
S3	K + 5% EO	95	5	0	0	2.432		SEM-EDX
S4	K + 9% EO	91	9	0	0	2.282		
S5	K + 3% EO + 10% FA	87	3	10	0	2.475		
S6	K + 3% EO + 25% FA	72	3	25	0	2.418		
S7	K + 3% EO + 45% FA	52	3	45	0	2.347		
S8	K + 5% EO + 10% FA	85	5	10	0	2.395		
S9	K + 5% EO + 25% FA	70	5	25	0	2.342		
S10	K + 5% EO + 45% FA	50	5	45	0	2.275		
S11	K + 9% EO + 10% FA	81	9	10	0	2.250		
S12	K + 9% EO + 25% FA	66	9	25	0	2.203		
S13	K + 9% EO + 45% FA	46	9	45	0	2.143		
S14	K + 3% EO + 25% FA + 0.04% NG	71.96	3	25	0.04	2.419		
S15	K + 3% EO + 25% FA + 0.08% NG	71.92	3	25	0.08	2.418		
S16	K + 3% EO + 25% FA + 0.12% NG	71.88	3	25	0.12	2.417		
S17	K + 5% EO + 25% FA + 0.04% NG	69.96	5	25	0.04	2.343		
S18	K + 5% EO + 25% FA + 0.08% NG	69.92	5	25	0.08	2.342		
S19	K + 5% EO + 25% FA + 0.12% NG	69.88	5	25	0.12	2.341		
S20	K + 9% EO + 25% FA + 0.04% NG	65.96	9	25	0.04	2.203		
S21	K + 9% EO + 25% FA + 0.08% NG	65.92	9	25	0.08	2.202		
S22	K + 9% EO + 25% FA + 0.12% NG	65.88	9	25	0.12	2.201		

*Gmix represents the specific gravity of the mixtures and is calculated using the weighted average of the specific gravities of the individual components, according to the following expression: Gmix = Gkaolinx(Kaolin ratio) + GEOx(EO ratio) + GFAx(FA ratio) + GNGx(NG ratio).

(3%). Furthermore, mixtures with higher EO content (*e.g.*, 9%) demonstrated even lower Gmix values when combined with FA, reaching as low as 2.143 for the 45% FA mix (S13). This confirms the compounding effect of EO and FA in reducing the unit weight of the blend.

In contrast, the addition of NG in small dosages (0.04–0.12%) had a negligible impact on Gmix. Across all NG-modified samples (S14–S22), the specific gravity remained almost constant for a given EO-FA composition, with changes observed only in the fourth decimal place. This indicates that the low dosage and high surface area of NG contribute insignificantly to the bulk density of the mixtures.

2.2.1 Sample preparation

The contamination and stabilization procedures of the kaolin samples were conducted following the methodology outlined below:

(i) The desired level of contamination was achieved by mixing the calculated weight percentage of the engine oil waste into the kaolin in predetermined proportions (0, 3, 5, and 9%). The kaolin–waste engine oil mixture was manually pulverized and thoroughly mixed in a sealed tray for 1 h (Figure 5a).
(ii) The mixture was then placed in a sealed container and allowed to equilibrate for a specified period, enabling the waste engine oil to distribute evenly within the kaolin.
(iii) Water was added to the kaolin–engine oil mixtures with varying degrees of contamination based on the optimum water ratios determined through Proctor tests.
(iv) Dry fly ash (10, 25, and 45%) was incorporated into the kaolin–waste engine oil mixtures at the predetermined weight ratios after specific contamination levels and times.
(v) Water was added according to the optimum water content determined by Proctor tests for the contaminated kaolin samples containing fly ash.
(vi) The mixtures were sealed in plastic bags for 24 h, after which the water content was rechecked before molding the samples.
(vii) For the addition of nanographene, the same steps as items (i)–(iv) were followed. A fixed amount of 25% fly ash was added, and the samples were prepared.

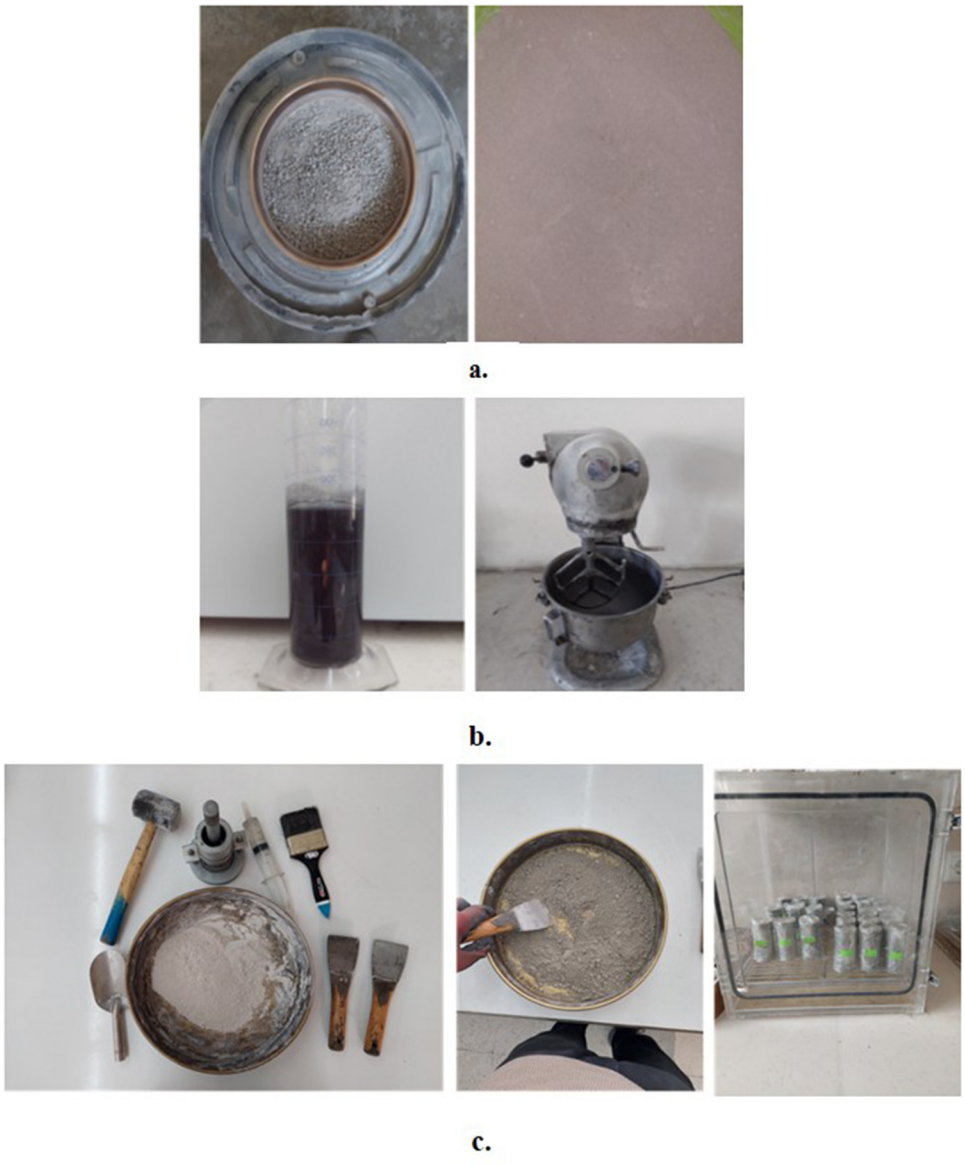

Figure 5: Preparation of the soil samples. (a) the kaolin-waste engine oil mixture, (b) nanographene solution, and (c) contamination process and test specimens.

The fly ash content was fixed at 25% by weight of the total binder in all nanographene-treated mixtures, based on preliminary optimization studies and previous literature reports, which indicated that this level of replacement provides a good compromise between strength development and durability performance when combined with nanomaterials.

(viii) A solution containing nanographene was prepared by mixing specific proportions of nanographene with the required amount of water using a mixer for 30–45 min (Figure 5b). To ensure uniform distribution of nanographene (NG) in the soil matrix and to minimize agglomeration, a mechanical mixing method was adopted. The required amount of NG was mixed with the calculated amount of water using a mechanical stirrer for 30–45 min (see Figure 5b). This process helped to disperse the NG particles evenly within the liquid medium and reduce clustering tendencies. The resulting NG suspension was then used as the mixing water in the Proctor tests (Step ix), and gradually added to the kaolin–waste engine oil–fly ash mixture in Step (x). Immediate and thorough manual mixing was conducted to ensure homogeneous distribution of the nanographene within the soil matrix and to further minimize the risk of re-agglomeration.

(ix) Proctor tests were performed using the solutions prepared for the kaolin–waste engine oil–fly ash mixtures, and water was added according to the optimum water content determined.
(x) The samples were prepared by incorporating nanographene into the kaolin–waste engine oil–fly ash mixture, with the nanographene added in proportions established based on the water content obtained.
(xi) The samples were then kept for specified durations of 0 and 7 days after contamination, and subsequently molded (Figure 5c).

2.2.2 Unconfined compression strength test (UCS) procedure

Determining the UCS of soils is crucial for addressing significant engineering issues such as bearing capacity, stability, and foundation design of structures. In order to evaluate the mechanical properties, UCS tests were conducted on kaolin samples contaminated with waste engine oil and stabilized with fly ash and NG. The UCS test was conducted in accordance with the ASTM D2166 [55] standards. The UCS of the samples was measured using a triaxial test machine at the Soil Mechanics Laboratory, Civil Engineering Department, Faculty of Technology, Firat University. A strain rate of 0.760 mm per minute was applied to apply the load on the specimens. The loading process was repeated until either the specimen failed or the strain reached 20% (as illustrated in Figure 6).

All soil specimens were prepared as 38 mm diameter and 76 mm high columns. The waste engine oil content was varied at different ratios based on the dry soil weight. The mixtures were compacted into three layers. The procedure for preparing the specimens and an overall view of the test machine are presented in Figures 5c and 6, respectively.

2.2.3 Microstructural analysis (SEM-EDX images)

The examination of the microstructural properties in soils requires the use of a crucial tool known as the scanning electron microscope (SEM) with the Thermo dispersive X-ray spectrometer (EDX), which offers high-resolution imaging capabilities. The advantages of SEM in the analysis of soil microstructure have led to its widespread application in the study of clays [56,57]. The microstructural analyses in this study were conducted at Marmara University's Nanotechnology and Biomaterials Application and Research Center. Scanning electron microscope images were obtained using the Zeiss EVO MA10 device available at the university (Figure 7). The soil samples were individually processed into powder form and then packaged. Images were captured at different magnification levels using the SEM device. Additionally, EDX analysis was performed on the same samples.

3 Results and discussions

3.1 Effect of fly ash and nanographene on the physical properties of kaolin contaminated with waste engine oil

The physical properties of kaolin clays can undergo changes when contaminated with waste diesel engine oil, including reduced water holding capacities, plasticity, and optimum water content. However, the extent of these

Figure 6: Unconfined compression strength (UCS) testing performed using a triaxial apparatus.

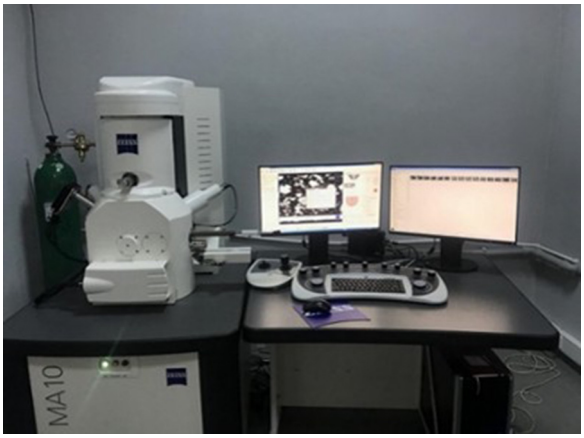

Figure 7: Scanning electron microscope.

changes can vary depending on the amount of waste oil and the specific properties of the kaolin clay. To complement the understanding of how contamination alters the mechanical behavior of kaolin, Figure 8 presents the stress–strain behavior of pure and EO-contaminated kaolin specimens. As seen in the figure, the addition of waste engine oil leads to a notable reduction in unconfined compressive strength (UCS) and a shift in peak strain, indicating a loss in stiffness and strength with increasing oil content. This mechanical degradation highlights the necessity for stabilization using materials such as fly ash and nanographene, which are discussed in the following section.

The alterations in the physical properties of kaolin clays, influenced by different degrees of contamination and the addition of various types and ratios of additives, are illustrated in Figure 9. The contamination of kaolin clays with waste diesel engine oil typically results in certain changes in their physical properties. The physical properties tests were conducted on samples that followed the 0-day contamination- that is, the tests were performed immediately after mixing the kaolin soil with the designated percentages of waste engine oil. The liquid limit of contaminated kaolin clays tends to increase, primarily due to the reduction in the water absorption capacity caused by the presence of waste oil. Consequently, the contaminated clays require more water to reach their liquid limit, leading to an increase in this parameter. In addition, the plasticity of kaolin is generally reduced when contaminated with waste diesel engine oil. This decrease in plasticity can be attributed to the decreased water absorption capacity of the clay caused by the waste oil. As a result, the contaminated clay exhibits a diminished ability to change shape and lower plasticity.

The physical properties of kaolin clays contaminated with waste diesel engine oil can vary depending on various factors. However, overall, there is typically a decrease in values such as moisture holding capacity and plasticity due to the reduction in water absorption capacity caused by the presence of waste oil in the kaolin clays. Previous studies have shown that the addition of fly ash has a notable impact on the compaction characteristics of contaminated kaolin clays [58–60]. A study by Ahmed [61] also demonstrated a decrease in w_{opt} values of soil up to the addition of 15% fly ash, followed by an increase.

Additionally, the maximum liquid limit (LL) value was observed at 10% fly ash addition for soil samples

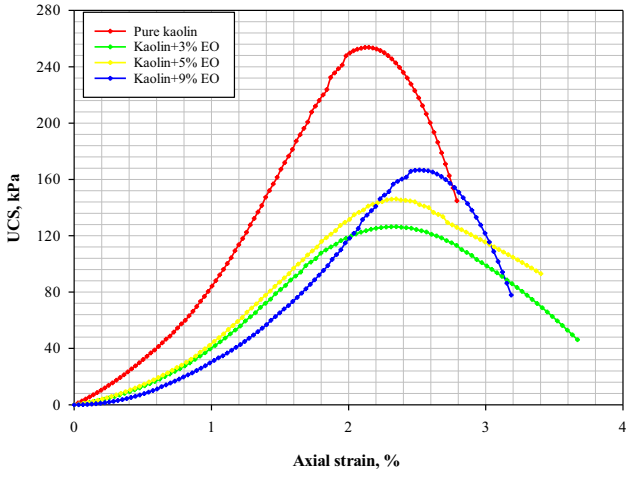

Figure 8: Stress–strain behavior of kaolin clay with varying content of contamination.

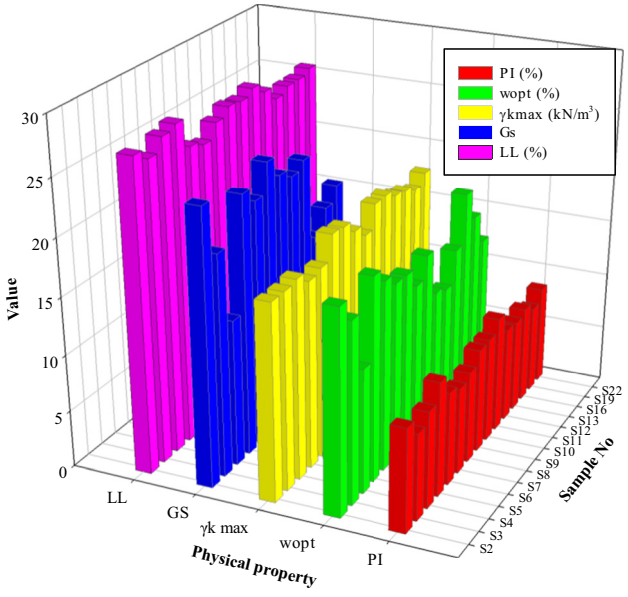

Figure 9: Changes in the physical properties of kaolin clays with varying degrees of contamination and the addition of different types and ratios of additives.

contaminated with 3% waste engine oil, the maximum plastic limit (PL) value was observed at 5% waste engine oil, and the maximum plasticity index (PI) value was observed at 9% waste engine oil. Furthermore, the maximum LL and PI values at 25 and 45% fly ash addition were determined for soil contaminated with 5% waste engine oil.

On the contrary, the introduction of nanographene to kaolin clays contaminated with waste diesel engine oil leads to alterations in certain physical properties of the material. The incorporation of nanographene enhances the mechanical properties of the material, particularly its compressive strength. These modifications may differ depending on the amount of nanographene used and the level of oil contamination present. Furthermore, when nanographene was added, the maximum values for LL and PI were attained in soils contaminated with 9% EO.

Consistent outcomes were observed in the soil contaminated with waste engine oil, primarily because of the structural transformation of the used kaolin clay. The absorption capacity of kaolin clay contaminated with waste engine oil was found to be satisfactory, with no significant changes in values occurring with the inclusion of additional materials in the kaolin clay.

3.2 Effect of fly ash and nanographene on the compaction characteristics of kaolin contaminated with waste engine oil

The compaction behavior of soils plays a significant role in determining their suitability for engineering applications, especially in cases involving contamination. In this study, standard Proctor compaction tests were performed on pure kaolin, oil-contaminated kaolin, and contaminated kaolin stabilized with fly ash (FA), nanographene (NG), and their combinations. The influence of waste engine oil (EO) contamination and the subsequent amendments on the maximum dry density (MDD) and optimum moisture content (OMC) was systematically investigated.

As shown in Figure 10, the optimum water content of contaminated kaolin clays is typically lower. The reduced water absorption capacity resulting from the waste oil contamination decreases the optimum water content level required for optimal compaction. The maximum dry unit weight of the contaminated kaolin clays tends to increase. This increase can be attributed to the reduced water absorption capacity caused by the waste oil, which subsequently raises the dry unit weight of the kaolin clay.

Two different scenarios were observed in relation to the addition of fly ash. First, as the fly ash content increased in the soil contaminated with 3% waste engine oil, the optimum water content (w_{opt}) values decreased. This phenomenon is consistent with previous findings in the literature, which indicate that the addition of fly ash decreases the w_{opt} values in soils [62,63]. In the second scenario, the lowest w_{opt} value for soil contaminated with 5 and 9% waste engine oil was observed at 25% fly ash addition. The increase in waste engine oil content is associated with substantial changes in the soil's properties. In soils where w_{opt} values decreased with increasing waste engine oil content, an increase in w_{opt} was observed after a certain fly ash content.

Further improvement in compaction behavior was achieved by incorporating nanographene into the fly

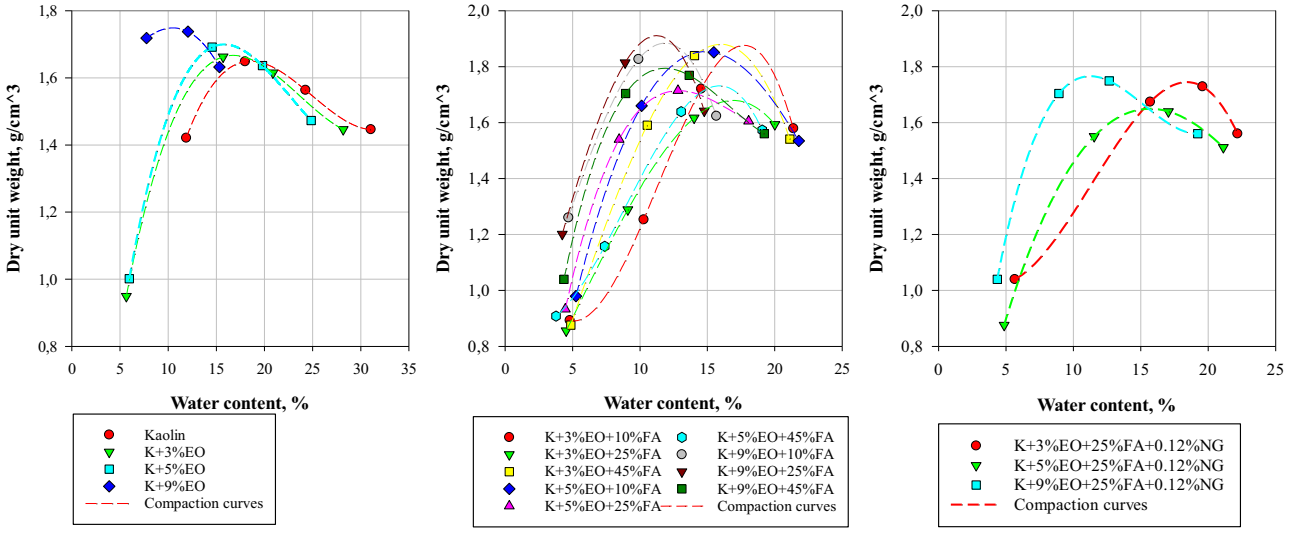

Figure 10: Compaction parameters of kaolin clays with varying degrees of contamination and the addition of different types and ratios of additives.

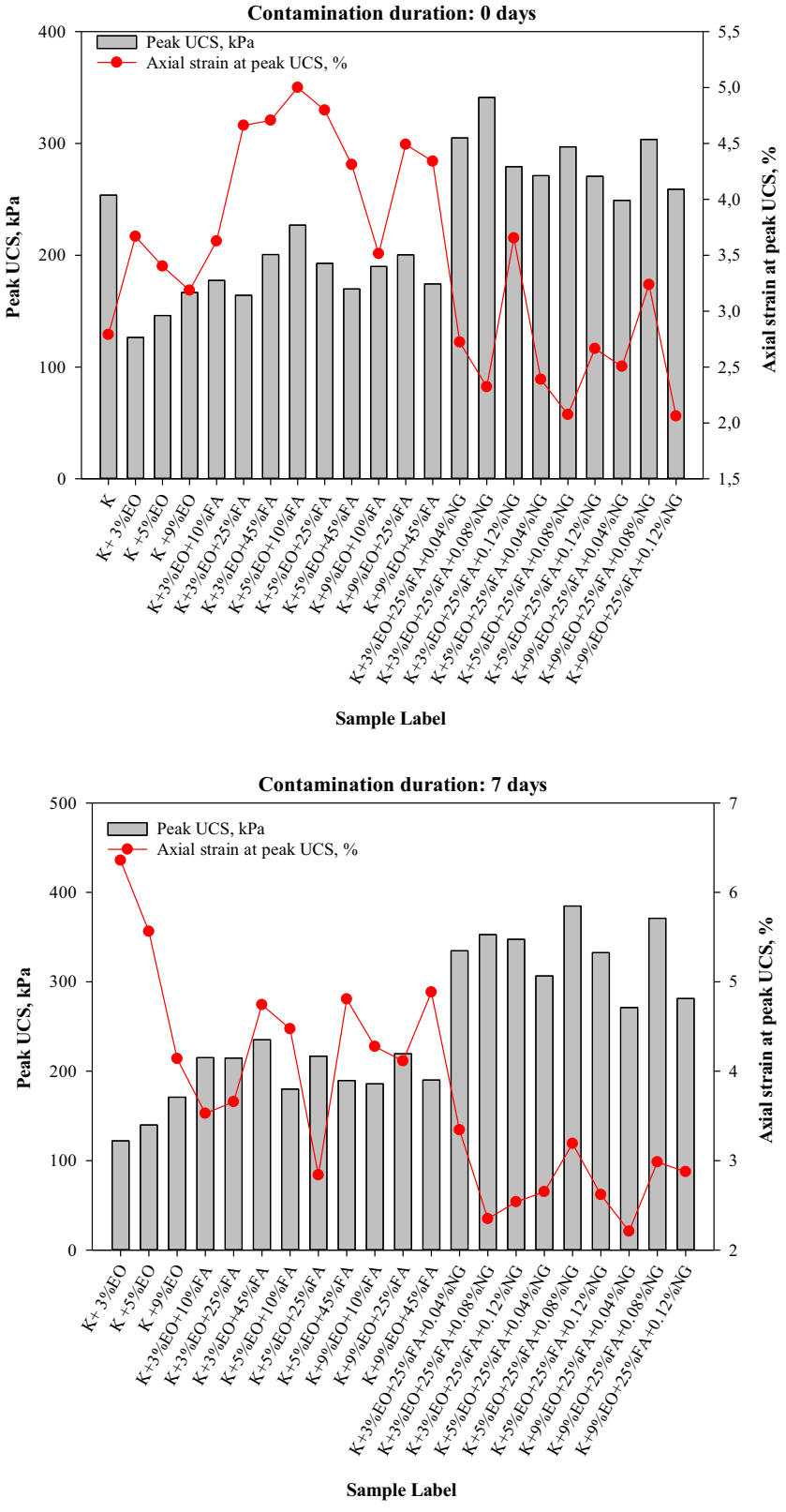

Figure 11: UCS Peaks and the axial stresses at the peak UCS of the samples for different contamination durations.

ash–stabilized mixtures. The curves showed an increase in maximum dry unit weight and a shift toward lower optimum moisture content. These enhancements are attributed to the high surface area and mechanical reinforcement properties of nanographene, which support a more compact and stable soil structure. The sharper peaks in the compaction curves indicate a more defined and responsive compaction behavior, suggesting a higher degree of structural ordering.

3.3 UCS performance of contaminated kaolin and stabilized contaminated kaolin with additives

Figure 11 illustrates the peak values of the unconfined compression strength and axial strains at the peak UCS for the pure kaolin samples with varying degrees of contamination, as well as the contaminated kaolin and stabilized contaminated kaolin samples incorporating different proportions of fly ash and nanographene. The results indicated that the degree of contamination significantly affects the unconfined compression strength. The UCS value of the contaminated kaolin samples exhibited a decrease compared to the pure kaolin samples due to the alteration in the structure caused by the presence of waste engine oil. Specifically, the reduction in UCS relative to uncontaminated kaolin was found to be 50.19% for samples with 3% engine oil, 42.12% for those with 5%, and 34.32% for samples with 9% engine oil content. This trend indicates a partial recovery of strength at higher contamination levels. Correspondingly, the UCS increased with higher waste oil content, in line with an observed increase in the maximum dry density of the samples.

Previous studies have demonstrated that, in addition to the degree of contamination, the unconfined compressive strength gradually decreases during the duration of

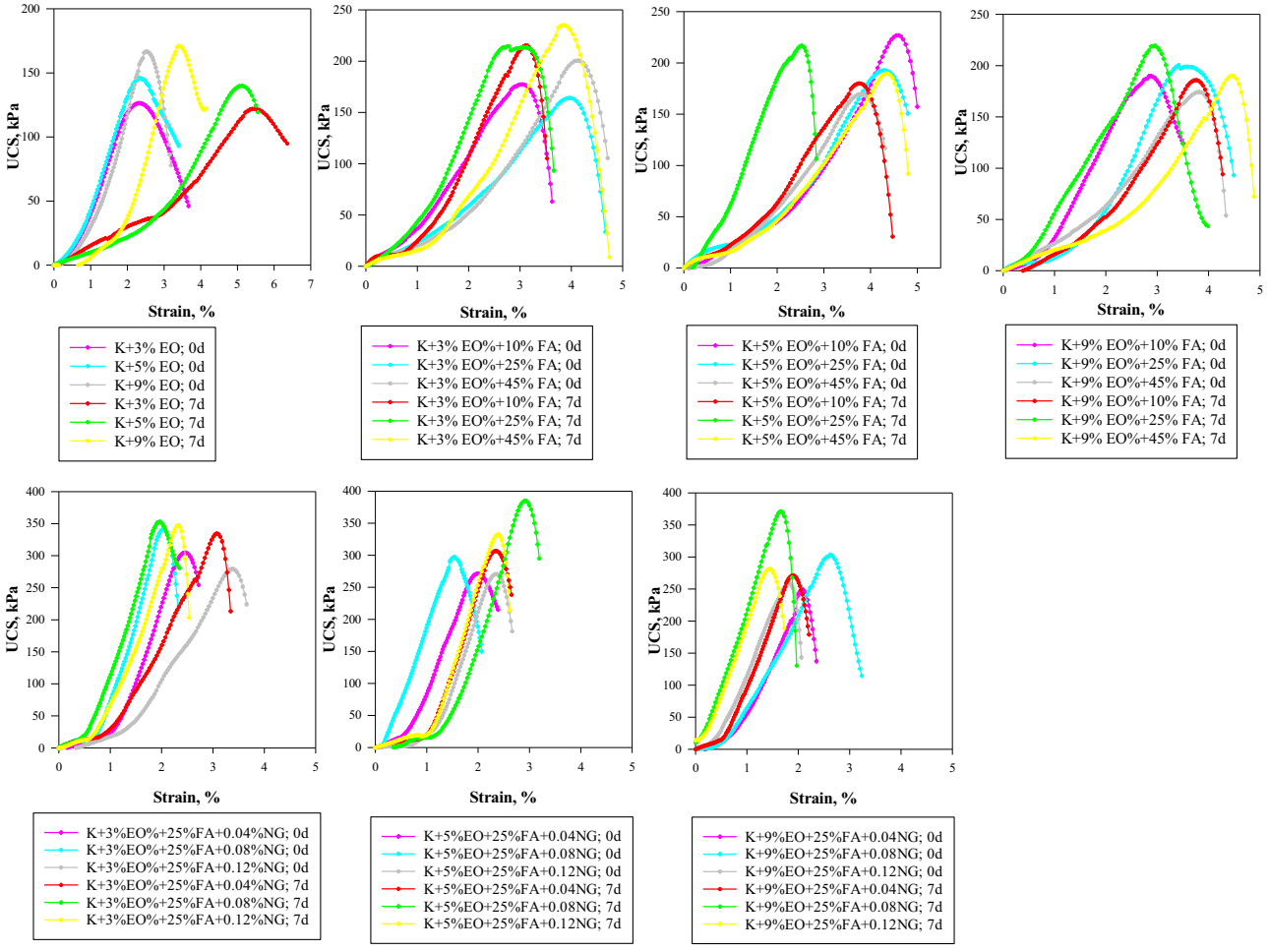

Figure 12: Stress–strain curves of kaolin samples contaminated with waste engine oil and treated with fly ash and nanographene for different contamination durations.

contamination and stabilizes at a constant value after a certain duration of contamination [64–66]. In this study, the UCS results were compared at two time points: the initial contamination (0 days) and after a 7-day contamination duration. Notably, no significant reduction in UCS values was observed for the samples contaminated for 7 days compared with the 0-day contamination samples. This can be attributed to the fact that it takes more than 7 days for the structural changes to occur in the kaolin clay due to the presence of the waste engine oil. Nazir [64] discovered in their research that the most significant impact on strength parameters occurred in samples exposed to a 6-month contamination period. Furthermore, the presence of additives led to a more pronounced increase in the UCS strength for the 7-day samples compared to the control groups.

The strength of the waste engine oil–kaolin mixtures exhibited enhancement as the proportion of fly ash was increased. When the contaminated kaolin samples were stabilized with varying ratios of fly ash, the influence of fly ash was more prominent in the samples contaminated with 3% oil, particularly at higher fly ash ratios. The addition of 45% fly ash resulted in a 58.62% improvement in the UCS strength of the contaminated kaolin sample. Conversely, the most significant improvement effects were observed at lower additive ratios in the kaolin samples with 5 and 9% waste engine oil additives.

At the end of the 7-day contamination duration, when the contaminated kaolin samples were stabilized with different fly ash ratios, the highest impact of increased fly ash ratio was observed in the samples with a 3% contamination degree. Specifically, the incorporation of 45% fly ash led to a 92.63% increase in the UCS strength of the 7-day contaminated kaolin sample. Similarly, the most pronounced improvement effects were observed in the samples exposed to contamination for 7 days, with a fly ash ratio of 25% in the 5 and 9% waste engine oil-added kaolin samples.

Furthermore, as the degree of contamination increases, the kaolin samples attain their maximum UCS values at lower strain rates. Moreover, when the contaminated kaolin samples were stabilized with fly ash, they reached their peak UCS values at relatively higher strain rates as the applied loading increased. This change in axial strain can be attributed to the distortion of the soil grains, enabling them to accommodate higher strain rates by rearranging the voids within the soil.

Conversely, at the end of the 7-day contamination duration, the contaminated kaolin samples exhibited similar behavior to the control samples, but an increase in the axial strain values at 7 days was observed. When the contaminated kaolin samples were stabilized with 10 and 25% fly ash, a decrease in the axial strain values was observed compared to the control groups. However, the contaminated samples stabilized with 45% fly ash reached their maximum UCS values at higher axial strains.

In this study, the maximum UCS values were achieved when 25% fly ash was used for stabilizing the contaminated kaolin samples. Therefore, 25% fly ash was incorporated as a binder in the soil samples along with the addition of nanographene, aiming to achieve the highest possible improvement in their strength. It was observed that the addition of fly ash and nanographene to the soil samples contaminated with different ratios resulted in a significant increase in the UCS strength, reaching the maximum rate of improvement. Specifically, the highest increase rate was observed with the addition of 0.08% nanographene in specimens contaminated with 3, 5, and 9% engine oil (169.74, 103.23, and 82.17%, respectively). Interestingly, the UCS values obtained for the maximum amount of nanographene (0.12%) were lower than those for the 0.08% nanographene addition.

In the study, considering the given boundary conditions, the optimum rate for the 0-day contamination duration was determined as 0.08% nanographene addition. However, for a contamination period of 7 days, the maximum UCS values were achieved when 25% fly ash and nanographene were added. The maximum increase rates in the UCS values for the samples contaminated with 3, 5, and 9% waste engine oil were 188.91, 174.96, and 117.14%, respectively, with the addition of 0.08% nanographene. This significant enhancement in UCS at the combination of 25% fly ash and 0.08% nanographene can be attributed to the synergistic interaction between the pozzolanic reaction of fly ash and the nano-reinforcement effect of graphene. The 25% fly ash ratio provides an optimal level of calcium-rich phases that react with the alumino-silicate components in the kaolin to form cementitious compounds such as calcium silicate hydrates (C–S–H), leading to a denser and stronger soil matrix. Simultaneously, the incorporation of 0.08% nanographene improves particle bonding and bridges micro-cracks due to its high surface area and mechanical strength, thereby enhancing the load transfer capacity and delaying the onset of failure. Higher graphene dosages (*e.g.*, 0.12%) may have resulted in agglomeration, reducing their effectiveness. Therefore, the selected dosages represent an optimal balance between chemical stabilization and physical reinforcement, producing the maximum improvement in the geotechnical performance of the contaminated kaolin.

3.4 Brittle index (IB) of contaminated kaolin and stabilized contaminated kaolin with additives

The addition of fly ash and nanographene to the contaminated kaolin samples had a significant impact on the peak behavior of the unconfined compression strength and led to changes in the brittleness behavior. To better illustrate the changes in the mechanical response of kaolin samples contaminated with waste engine oil and treated with fly ash and nanographene, stress–strain curves were presented in Figure 12. These curves provide a clearer understanding of the variations in peak strength and the transition in brittleness behavior observed during the UCS testing. The graphical representation supports the discussion by revealing the ductile or brittle nature of the treated and untreated samples under axial loading.

In order to elucidate the ductile and brittle characteristics of the samples, the calculated values using the brittleness index (IB) formula, as presented in equation (1), are depicted in Figure 13.

$$\mathrm{IB} = \frac{q_{\mathrm{f}}}{q_{\mathrm{ult}}} - 1. \tag{1}$$

Inhere q_{f} represents the failure UCS, and q_{ult} represents the ultimate UCS. As the values of IB approach zero, the samples exhibit a more ductile failure behavior in the stress–strain curves [67].

According to Figure 13, the samples exhibited a more brittle behavior as the brittleness index values deviated from zero, indicating an increase in the contamination rates of the kaolin samples. The brittleness index of the samples increased by 51.74% at the maximum contamination degree for a 0-day duration. Additionally, based on the brittleness index results, the utilization of 45% fly ash contributed more to the ductile behavior of the kaolin samples with 3 and 5% contamination degrees, whereas it caused a more brittle behavior in the kaolin samples with a 9% contamination degree. Notably, the samples displayed more ductile behavior when employing lower percentages of fly ash in the kaolin samples with a 9% contamination degree.

After the 7-day contamination duration, the stress–strain curves of the samples demonstrated a more ductile behavior with increasing contamination degrees of the kaolin samples. Moreover, when the contaminated samples were stabilized with 45% fly ash, the kaolin samples with a 3% contamination degree exhibited more brittleness compared to the samples with 5 and 9% contamination degrees. This can be attributed to the fact that the presence of fly ash within the soil structure alters the kaolin structure to a greater extent in cases with lower contamination

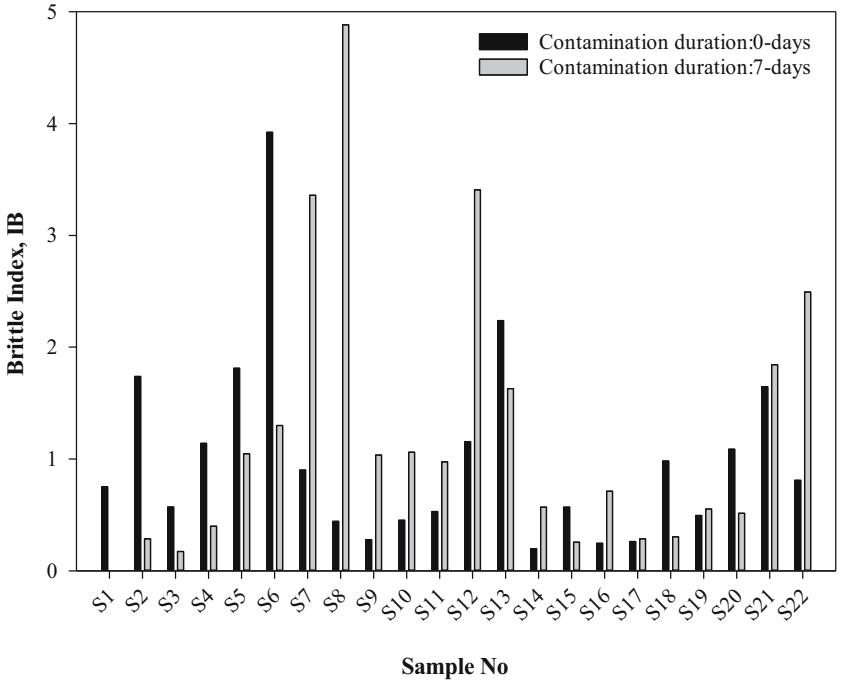

Figure 13: Changes in the brittle index of the samples for 0-day and 7-day.

degrees. Conversely, the behavior observed in the stress–strain curves with lower percentages of fly ash in the kaolin samples with a 9% contamination degree resembles that of the samples with a 0-day contamination duration.

In the nanoenhanced specimens, it was determined that specimens containing 0.08% nano-additives exhibited a more brittle behavior. In other ratios, the brittleness index values of the specimens were below zero, indicating

Figure 14: Fracture modes of the samples for 0 and 7 days curing period.

a more ductile behavior in the stress–strain curves compared to specimens with lower and higher nano-additive content.

On the contrary, increasing the degree of contamination of the specimens and adding nanographene resulted in a more brittle behavior in the stress–strain curves. Changes in the exhibited behaviors of the specimens were observed after a 7-day contamination period. Specimens with a higher percentage of nano-additives demonstrated a more brittle behavior for all contamination degrees. Hence, the addition of nanomaterials has increased the brittleness of the materials as the degree of contamination increases.

3.5 Failure modes and SEM–EDX images of the samples

Figure 14 illustrates the failure modes observed through visual observation following the UCS test. These failure modes can vary based on the structural characteristics of the kaolin clay, the degree of contamination, the stabilization rate, and the contamination duration. Understanding these failure modes is crucial for comprehending the behavior and strength properties of the samples. The failure modes observed in the kaolin clay samples after the UCS test include surface failure, internal failure, and shear banding.

Based on the information provided in Figure 14, the failure mode of the kaolin samples under unconfined compression strength is influenced by the degree of contamination, the duration of contamination, and the amount of additives. For a low contamination degree (3% EO), a single conical shear plane is formed, whereas an increase in the contamination degree leads to a vertically developed failure mode. Furthermore, the failure modes become more pronounced with longer contamination durations and the addition of fly ash, which is characterized as an internal fracture. In this failure mode, the failure propagates deep into the sample, typically occurring in structurally weak regions or at junction points within the sample.

In the case of nanoreinforced kaolin samples, distinct failure surfaces were not observed as clearly as in the contaminated kaolin samples and the contaminated and fly ash–stabilized samples. The failure modes observed in these samples included surface cracks and shear banding. Shear banding occurs when distinct zones of concentrated shear stresses form within the sample due to the stress concentration.

Prior to SEM analysis, representative samples of pure kaolin, contaminated kaolin (with waste engine oil), and stabilized kaolin mixtures were oven-dried at 40°C to avoid thermal alteration of microstructures. The dried specimens were then gently ground into fine powder and mounted onto aluminum stubs using carbon tape. Subsequently, the samples were gold-coated to enhance conductivity and prevent charging during imaging.

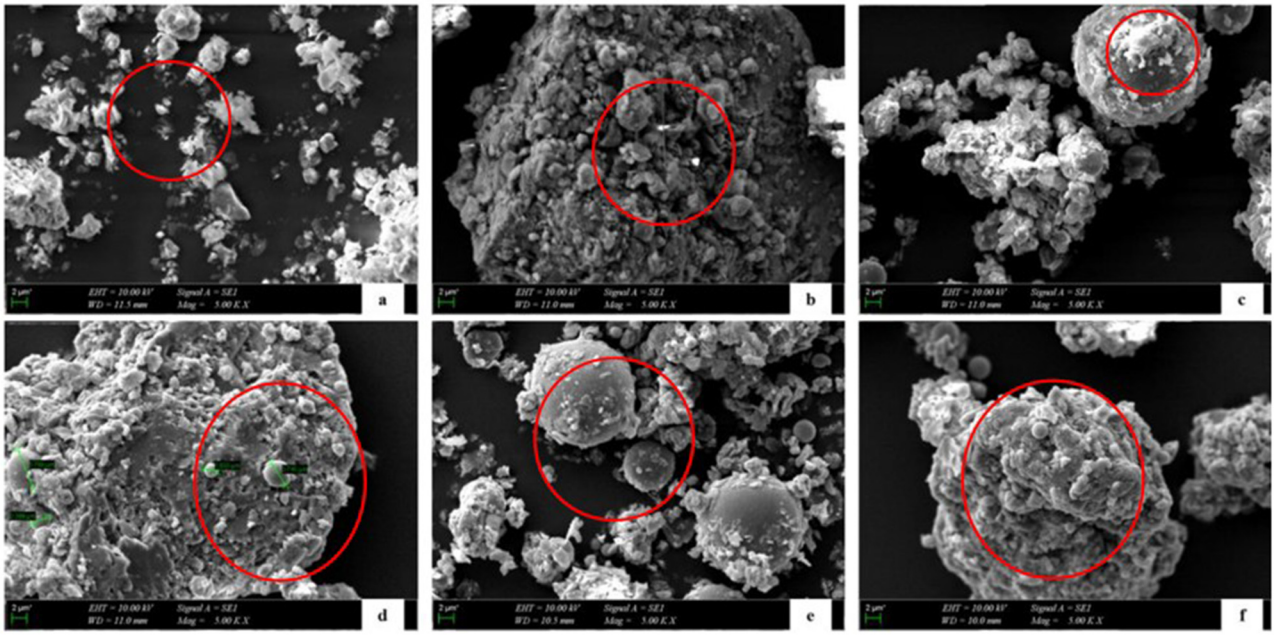

Figure 15: SEM Images of the samples (a: Kaolin; b: K + 9% EO; c: K + 3%EO + 45%FA; d: K + 3%EO + 45%FA (emphasizing separation of oil agglomerates); e: K + 3%EO + 25%FA + 0.12% NG; f: K + 9%EO + 25%FA + 0.12% NG).

SEM was used to characterize the morphological and structural features of the pure kaolin, waste engine oil-contaminated kaolin, and stabilized kaolin clays. As shown in Figure 15a, the SEM image of the pure kaolin reveals a loose and irregularly agglomerated morphology with particle sizes ranging between 2 and 20 μm. The red circle highlights clusters of kaolinite particles with weak interparticle bonding, indicating high porosity and an undisturbed clay structure. In contrast, Figure 15b, which represents kaolin contaminated with 9% waste engine oil, shows a compact, flake-like structure as marked in the red circle. The oil binds the soil particles closely through van der Waals and hydrogen bonding, forming a dense and cohesive matrix. This morphological change supports the increase in plasticity and reduction in permeability typically observed in contaminated clays.

Figure 15c presents a kaolin sample contaminated with 3% engine oil and stabilized with 45% fly ash. The circled region in the image displays rounded and more discrete particles, resembling the morphology of pure kaolin. This indicates that the fly ash has improved particle dispersion and partially restored the microstructure by mitigating the oil's binding effect.

The SEM image in Figure 15d (with the same FA content) further emphasizes this effect. The red-circled zone clearly shows detachment of oil agglomerates from the kaolin surface. This separation suggests that the fly ash has not only physically diluted the oil but has also disrupted the oil-soil interaction, enhancing stabilization. Figure 15e represents the sample with 3% EO, 25% FA, and 0.12% nanographene. The highlighted region shows uniform, granular particles with smoother surfaces. The addition of nanographene appears to enhance bonding between particles and facilitate more effective removal of oil residues, as observed by the reduced oil clusters.

Lastly, in Figure 15f, where 9% EO, 25% FA, and 0.12% NG were used, the red circle illustrates a dense, restructured granule. Despite the higher EO content, the combined effect of FA and NG leads to a more compact and stabilized particle arrangement, indicating improved interaction and reduced contamination effects.

Figure 16 presents the surface elemental compositions obtained by EDX analysis of pure kaolin, soil contaminated with waste engine oil (K + 9%EO), and kaolin after remediation (K + 3%EO + 45%FA; K + 9%EO + 45%FA; K + 3%EO + 25%FA + 0.12%NG; K + 9%EO + 25%FA + 0.12%NG).

To better understand the microstructural characteristics observed in the SEM images, such as the formation of binding gels, particle agglomeration, and the dispersion of nanographene, it is essential to consider the interaction mechanism between the fly ash, nanographene, and the contaminated kaolin matrix. This interaction mechanism is visually summarized in Figure 16, where the microstructural synergy between FA and NG within the contaminated kaolin matrix is illustrated. The conceptual model highlights the complementary roles of the two additives and their contribution to the improvement of strength, density, and brittleness index.

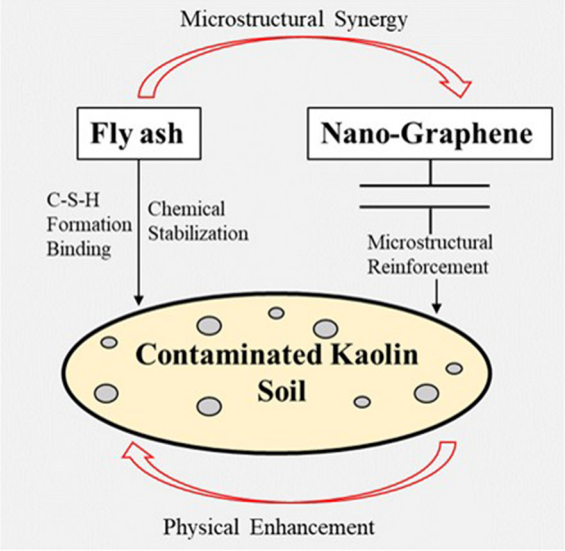

Figure 16: Conceptual illustration of the interaction mechanism between fly ash, nanographene, and waste engine oil-contaminated kaolin.

Fly ash, a pozzolanic material, reacts with calcium hydroxide ($Ca(OH)_2$) in the presence of water to form calcium silicate hydrate (C–S–H) gels, which serve as the primary binding agents within the soil matrix. These reaction products fill the pore spaces, reduce permeability, and improve the overall cohesion and strength of the soil [68]. In EO-contaminated kaolin, which exhibits reduced bonding and increased brittleness, the formation of C–S–H helps reconstruct a stable soil skeleton by chemically binding the soil particles. Nanographene, on the other hand, does not exhibit pozzolanic or binding properties on its own. However, its high specific surface area, exceptional tensile strength, and ability to fill microvoids enable it to enhance the microstructure of the soil. When uniformly dispersed in the FA-stabilized matrix, NG improves stiffness and contributes to reducing microcracks and deformation under loading. Its effectiveness is maximized in a chemically stable and dense matrix, which is precisely provided by the pozzolanic reactions of fly ash. When both materials are used together, fly ash provides the necessary chemical environment and binder matrix that allows nanographene to be effectively integrated and anchored within the soil structure. The result is a dual-mechanism stabilization: FA ensures chemical bonding and structural solidification, while NG reinforces the matrix physically by enhancing load distribution and resisting fracture propagation.

As shown in Figure 17, the EDX analysis revealed the presence of Si, Al, K, S, and O in the pure kaolin. In the EDX analysis of the soil contaminated with waste engine oil, elements C, O, Si, and Al were detected to be dispersed within the kaolin. According to the EDX analysis results of the pure kaolin, contaminated kaolin, and stabilized kaolin, their main components were identified as Si, Al, and O. Changes in the content of these elements were characterized in the stabilization results, as most waste engine oil, based on ICP-MS analysis, comprised carbon and aluminum.

The aluminum content in the pure kaolin, which could be attributed to the organic matter, was found to be 17.62%. Due to the significant amount of waste oil in the contaminated kaolin, the carbon and aluminum percentages were found to be 12.39 and 17.82%, respectively. However, in the stabilized samples, lower values of carbon and aluminum were observed compared with the other contents. This indicates that the stabilization products used greatly reduced the impact of the engine oil waste, leaving only a small amount of residue in the kaolin sample.

3.6 The secant modulus (E_{s50}) of contaminated kaolin and stabilized contaminated kaolin with additives

The secant modulus (E_{s50}), which represents the average stiffness of the soil, is a crucial design parameter for soil materials. It is determined by calculating the ratio of the axial stress to the corresponding axial strain at a specific point on the stress–strain curve. In other words, the secant modulus is defined as the slope of the curve from zero deviator stress to deviator stress, which is half or one-third of the peak deviator stress [69–72]. In this study, the secant modulus was computed for each sample using the point corresponding to 50% of the sample's unconfined compression strength, as indicated in equation (2) [72,73]. Figures 18 and 19 illustrate the relationship between the secant modulus (E_{s50}) and various additive ratios for the contaminated kaolin samples.

$$E_{s50} = \frac{\Delta q_{50\%}}{\Delta \varepsilon_{50\%}}, \tag{2}$$

where $\Delta q_{50\%}$ is the value related to 50% of the sample's UCS, and $\Delta \varepsilon_{50\%}$ refers to the strain corresponding to half of the UCS of the sample.

According to the findings presented in Figure 18, the secant modulus of the kaolin samples that underwent 7-day contamination before stabilization was observed to be lower compared to the 0-day samples. In the case of samples exposed to 0-day contamination, an increase in the fly ash ratio increased the secant modulus. However, for samples with 3 and 9% contamination degrees, the secant modulus increased with a 10% addition ratio, while a decrease was observed with further increases in the fly ash ratio. On the other hand, in samples with a 5% contamination degree, the addition of fly ash resulted in a decrease at lower fly ash rates, but exhibited a slight increasing trend for higher ratios.

Additionally, the maximum secant modulus values for all contamination degrees of kaolin samples exposed

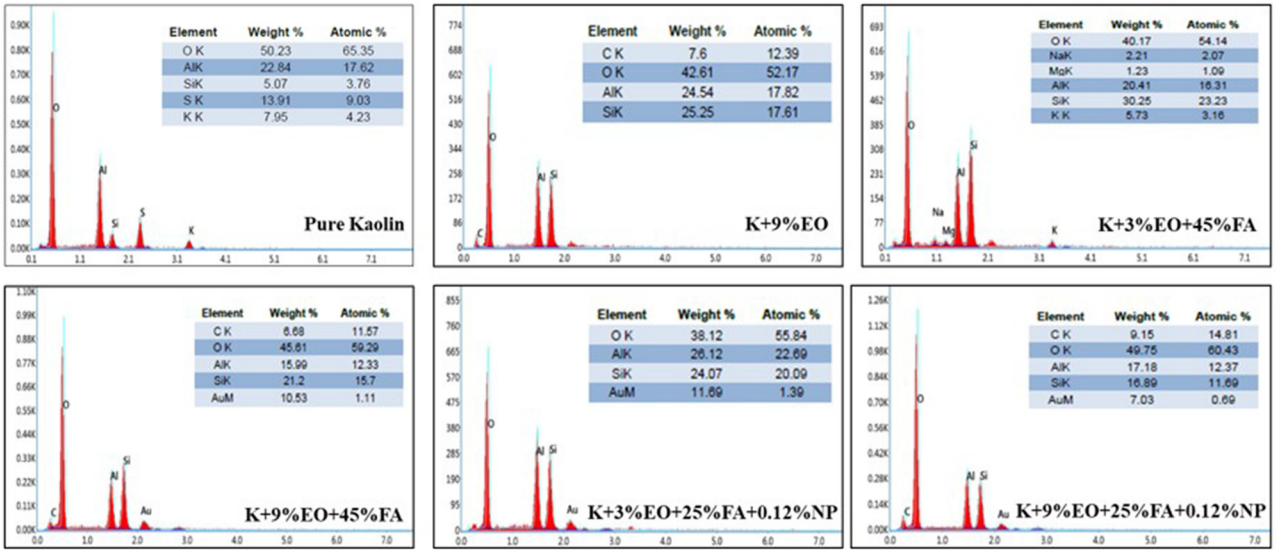

Figure 17: EDX analysis of the samples.

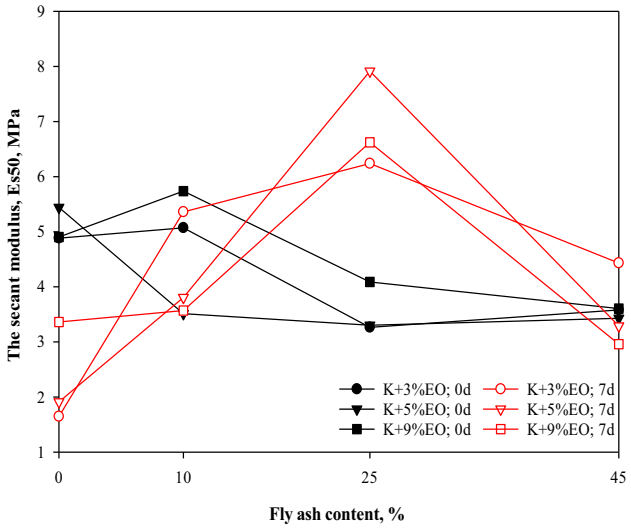

Figure 18: The secant modulus of the contaminated kaolin samples stabilized with fly ash for 0-day and 7-day.

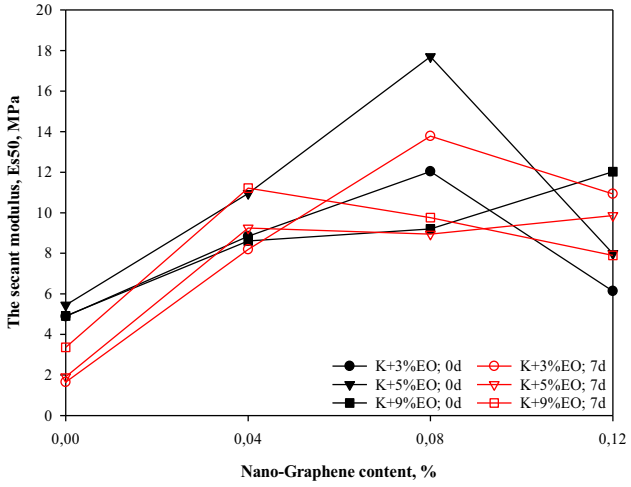

Figure 19: The secant modulus of contaminated kaolin samples stabilized with nanographene for 0-day and 7-day.

to 7-day contamination were observed when the fly ash ratio was 25%. The results also indicate that the E_{s50} value varies with changes in the fly ash content and the duration of contamination in kaolin samples contaminated with waste engine oil. Therefore, there exists an indirect relationship between E_{s50} values and these factors.

As shown in Figure 19, an increase of up to 0.08% nanographene before curing increased the secant modulus for 3 and 5% contamination levels, while increases after this rate decreased the secant modulus. It was determined that the secant modulus of the kaolin samples at the 9% contamination level increased gradually with the addition of nanographene. On the other hand, the secant moduli of the samples with 7-day curing increased up to 0.08% for all contamination levels and decreased after this rate. The observed reduction in the secant modulus (E_{s50}) when the nanographene content exceeds 0.08% can be attributed primarily to the tendency of nanographene particles to agglomerate at higher dosages. Agglomeration leads to poor dispersion of nanoparticles within the soil matrix, resulting in the formation of weak zones or defects that compromise the uniform stress transfer and mechanical reinforcement effects. Instead of enhancing particle bonding and load distribution, excessive nanographene clusters can create stress concentration points that reduce overall soil stiffness and strength. Moreover, higher nanoparticle content may increase the viscosity or hinder proper mixing, limiting the effective interaction between nanographene and soil particles.

The secant modulus (E_{s50}) is a key indicator of the stiffness and deformation behavior of soils under axial loading. In practical geotechnical engineering applications, it provides valuable insight into how much a soil will compress under given stress levels, which is essential for settlement predictions and deformation analysis of foundations, embankments, and pavements. In the context of this study, the E_{s50} values allow for the comparison of the initial stiffness of treated and untreated kaolin samples under different contamination and stabilization conditions. Higher secant modulus values indicate stiffer, more stable soils with reduced deformation potential, which is particularly desirable in contaminated soil environments. Thus, tracking changes in E_{s50} with varying fly ash and nanographene dosages helps assess the effectiveness of each additive combination in enhancing soil stiffness, and supports the selection of optimal stabilizer content for practical field applications.

3.7 Optimization process of waste engine oil–contaminated soil stabilized with different additives

The Gray correlation analysis was employed in this study to investigate the effects of the degree of contamination, the mineral additive, and the nanoparticle stabilization on the mechanical properties of the kaolin clay. The objective was to optimize the strength properties of the contaminated kaolin clay. The study evaluated the relationships between the degree of contamination (associated with waste engine oil), the stabilization ratios of the additives, and the experimental outcomes such as the maximum

unconfined compression strength (q_u), brittle index (IB), and the secant modulus (E_{s50}). Each experimental output was treated as the reference sequence, while the contamination degree and stabilization ratios were considered as the comparison sequence. The following stages were employed in this study to determine the gray relational order and the gray relational degree. The reference sequence $f_o(m)$ in equation (3) represents the ideal values of the performance indicators (*i.e.*, maximum unconfined compressive strength, brittleness index, and secant modulus) used in this study. The comparison sequences $f_i(m)$ in equation (4) correspond to the experimental data obtained from different stabilization combinations and contamination levels. These equations form the basis for computing the gray relational coefficients and degrees, which ultimately allow for the ranking of samples and optimization of stabilization performance. Therefore, they play a critical role in interpreting and comparing multi-response outcomes within the GRA framework.

1) The following equations (3) and (4) describe the reference and comparison sequences $f_o(m)$ and $f_i(m)$, respectively:

$$f_0(m) = \{f_0(m_1), f_0(m_2), f_0(m_3), \ ..., \ f_0(m_n)\}, \quad (3)$$

$$f_i(m) = \{f_i(m_1), f_i(m_2), f_i(m_3), \ ..., \ f_i(m_n)\}. \quad (4)$$

2) To normalize and nondimensionalize the parameters that have different dimensions in the sequences, equations (5) and (6) were used.

$$f_0'(m) = f_0'(m)/f_0(m_1) = \{f_0'(m_1), f_0'(m_2), \ ..., \ f_0'(m_n)\}, \quad (5)$$

$$f_i'(m) = f_i'(m)/f_i(m_1) = \{f_i'(m_1), f_i'(m_2), \ ... \ f_i'(m_n)\}. \quad (6)$$

3) Eq. (7) computes the correlation coefficient, $\xi_i(m)$;

$$\xi_i(m) = \frac{\min_i \min_m |f_0(m) - f_i(m)| + \rho \max_i \max_m |f_0(m) - f_i(m)|}{|f_0(m) - f_i(m)| + \rho \max_i \max_m |f_0(m) - f_i(m)|}, \quad (7)$$

inhere ρ is the differentiating coefficient ($\rho \in [0, 1]$), which is typically set to 0, as it often provides strong stability while maintaining moderate differentiating effects [74].

4) Eq. (8) shows the gray correlation degree (r_i):

$$r_i = \frac{1}{n} \sum_{m=1}^{n} \xi_{0i}(m). \quad (8)$$

The proximity degrees ($|f_0(m) - f_i(m)|$) between the reference sequence and comparison sequence have been calculated from equation (6), and it was shown that $\min_i \min_m |f_0(m) - f_i(m)| = 0$ and $\max_i \max_m |f_0(m) - f_i(m)| = 1$.

Kaolin-type clays are commonly found in weak soils and typically exhibit poor bearing capacity. However, when these clays come into contact with contaminants such as waste engine oil, their essential properties, such as durability, water permeability, and soil stability, can be compromised. To address this issue, the use of fly ash and nanographene powder is effective in enhancing the geotechnical properties of contaminated kaolin-type clays.

In light of this, a gray correlation analysis was conducted to investigate the influence of parameters, including the degree of soil contamination, type of stabilization material, and percentage ratio, on various engineering properties such as the unconfined compressive strength, brittle index, and secant modulus of kaolin-type clay soil. The gray correlation ranks and gray correlation degrees are presented in Table 7 and Figure 20, respectively.

Based on the analysis presented in Table 7 and Figure 20, the gray correlation sequence for the q_f was determined to be CD > FA > NG for both the 0-day and 7-day contamination

Table 7: Gray correlation degrees (r_i)

Reference sequence	Parameter	Comparison sequence (0-day)			Comparison sequence (7-days)		
		CD	FA	NG	CD	FA	NG
q_u	r_i	0.6124	0.5780	0.4827	0.5641	0.5574	0.4487
	R	1	2	3	1	2	3
IB	r_i	0.6189	0.6572	0.6731	0.5460	0.6652	0.6103
	R	3	2	1	3	1	2
E_{s50}	r_i	0.6079	0.6653	0.6322	0.6209	0.6334	0.6064
	R	3	1	2	2	1	3

R: gray correlation ranks, q_u: unconfined compression strength at failure, IB: Brittle index, and E_{s50}: the secant modulus.

durations. It was found that the degree of contamination had a greater impact on the q_f compared to the type and proportion of the stabilization material, regardless of the duration of contamination. Fly ash, as a mineral material, was found to be more effective in improving the UCS strength of contaminated kaolin soils compared to nanographene powder.

Regarding the IB, the presence of the stabilization materials significantly influenced the behavior of the material. At the 0-day contamination duration, the gray correlation rank for IB was determined as NG > FA > CD. The presence of nanographene powder emerged as the primary parameter affecting the brittleness and ductility of the material. However, at the 7-day contamination duration, the gray correlation rank for IB was determined as FA > NG > CD. Fly ash exhibited the most significant effect on the brittle index of kaolin soils exposed to 7-day contamination.

The gray correlation order for the E_{s50} was found to be FA > NG > CD at the 0-day contamination duration. The presence of fly ash had the most significant impact on the strain rate in relation to the stress at 50% of the stress–strain curve of the material. At the 7-day contamination duration, the gray correlation order for E_{s50} was determined as FA > CD > NG. The degree of contamination had a greater influence on the secant modulus compared with the presence of nanographene.

Moreover, the maximum correlation coefficients, ξ_{max}, were observed as follows:

- For q_f at 0-day contamination: $\xi_{CD} = 0.9847$, $\xi_{FA} = 0.9847$, $\xi_{NG} = 0.6813$.
- For q_f at 7-day contamination: $\xi_{CD} = 0.9773$, $\xi_{FA} = 0.9946$, $\xi_{NG} = 0.7620$.
- For IB at 0-day contamination: $\xi_{CD} = 0.8844$, $\xi_{FA} = 0.9076$, $\xi_{NG} = 0.9553$.
- For IB at 7-day contamination: $\xi_{CD} = 0.8813$, $\xi_{FA} = 1.000$, $\xi_{NG} = 0.9190$.
- For E_{s50} at 0-day contamination: $\xi_{CD} = 0.9816$, $\xi_{FA} = 0.9576$, $\xi_{NG} = 0.9807$.
- For E_{s50} at 7-day contamination: $\xi_{CD} = 0.9887$, $\xi_{FA} = 0.9789$, $\xi_{NG} = 0.9229$.

Based on these results, the optimum combination for achieving the maximum unconfined compressive strength under the studied conditions is the use of 0.12% nanographene powder with 25% fly ash addition for kaolin samples contaminated with 5% waste engine oil. This combination helps mitigate the adverse effects of engine oil on the strength properties of kaolin. On the other hand, for the brittle index, the recommended optimum values are the addition of 10% fly ash and 0.04% nanographene powder for 3% engine oil contamination prior to the contamination period. After 7 days of contamination, 45% fly ash with 0.04% nanographene powder was used for 3% engine oil contamination. Regarding the secant modulus, the optimum combination for kaolin samples is 10% fly ash and 0.08% nanographene at 3% engine oil contamination for 0-day contamination, and 25% fly ash and 0.08% nanographene at 3% engine oil contamination after 7 days of contamination.

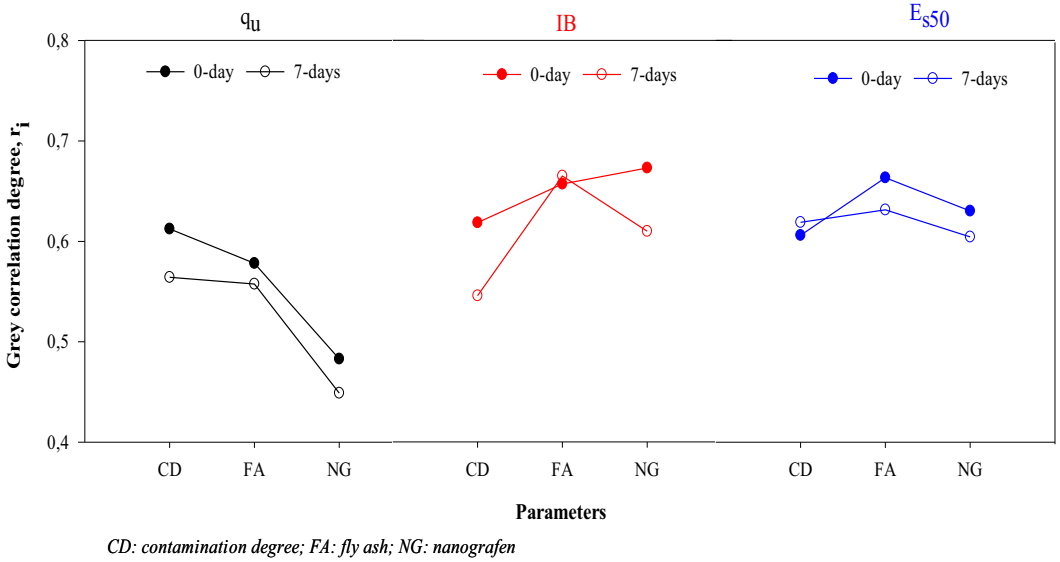

Figure 20: The r_i values of soil contamination, type, and percentage ratio of the stabilization material on the engineering properties of kaolin soil for 0 and 7 contamination durations.

4 Conclusions

In this study, the effects of NG and FA additives on the physical and engineering properties of kaolin clay contaminated with waste engine oil (EO) were investigated experimentally. Furthermore, the role of the contamination time on these properties was investigated, and the optimum additive rates were determined by Gray Relation Analysis (GRA). The main findings are summarized below:

- The physical properties of the soils showed an increase in liquid limits and a decrease in plasticity index due to EO contamination. The highest LL value was obtained with the combination of 10% FA and 3% EO, whereas the highest PI value was observed with 5 and 9% EO. The effect of NG doping varied depending on the amount of EO; NG doping increased LL and PI in samples treated with 9% EO.
- Proctor compaction results showed that EO decreased the optimum water content (opt) and increased the dry unit weight. FA addition decreased opt, while NG addition increased opt at all EO ratios compared to FA addition.
- EO contamination decreased soil strength; however, this negative effect was reversed by the addition of FA and NG additives. In particular, 45% FA admixture resulted in a 58.62% strength increase in the samples containing 5% and 9% EO. The highest UCS value was obtained with 0.08% NG.
- Although 45% FA exhibited a more ductile behavior at lower EO ratios, it increased brittleness at 9% EO. The NG admixture significantly increased the brittleness above 0.08%, causing brittle behavior at all EO levels.
- FA admixture generally increased the E_{s50} value. 25% FA provided the highest E_{s50} value after 7 days of contamination. NG doping increased E_{s50} up to 0.08%, whereas doping above this level led to a decrease (especially at 3 and 5% EO).
- The optimum additive combinations were determined according to the GRA analysis as follows:

o For UCS 5% EO → 25% FA + 0.12% NG
o For IB: 3% EO, 0 days → 10% FA + 0.04% NG; 7 days → 45% FA + 0.04% NG
o For E_{s50}: 3% EO, 0 days → 10% FA + 0.08% NG; 7 days → 25% FA + 0.08% NG

This study highlights the effectiveness of using a combined treatment of fly ash and nanographene in improving the geotechnical properties of kaolin clay contaminated with waste engine oil. The results showed that 25% fly ash and 0.08% graphene yielded optimal improvement in unconfined compressive strength, maximum dry density, and reduced porosity. For researchers and practicing engineers working in the field of contaminated soil remediation, these findings suggest a promising approach for stabilizing oil-contaminated fine-grained soils.

While the combined use of fly ash and nanographene has shown promising results in enhancing the geotechnical properties of contaminated kaolin soils under laboratory conditions, its field-scale application warrants further investigation. Particularly, the use of nanographene raises valid concerns related to environmental toxicity, leachability, and cost-effectiveness. Although the dosage used in this study was intentionally kept low (0.08%) to mitigate ecological risks, the long-term behavior and potential release of graphene particles into the environment remain areas of concern. Furthermore, the current high cost of graphene limits its immediate viability for large-scale soil stabilization projects. Future studies should focus on life cycle assessments (LCA), eco-toxicological evaluations, and the development of cost-efficient, scalable production methods for graphene, in order to ensure its safe and sustainable use in geotechnical engineering.

Acknowledgments: This study was supported by the Firat University (in Turkey) Science Research Projects (FUBAP) (Project no. TEKF.22.35 and TEKF.25.03). We appreciate the financial assistance from FUBAP.

Funding information: This study was supported by the Firat University (in Turkey) Science Research Projects (FUBAP; Project no. TEKF.22.35 and TEKF.25.03). We appreciate the financial assistance from FUBAP.

Author contributions: All authors have accepted responsibility for the entire content of this manuscript and approved its submission.

Conflict of interest: The authors state no conflict of interest.

Data availability statement: The datasets generated and/or analysed during the current study are available from the corresponding author on reasonable request.

References

[1] Ramadass K, Megharaj M, Venkateswarlu K, Naidu R. Ecological implications of motor oil pollution: Earthworm survival and soil

health. Soil Biol Biochem. 2015;85:72–81. doi: 10.1016/J.SOILBIO.2015.02.026.
[2] Mojtahed Sistani SV, Negahdar H, Bamoharram FF, Shakeri MR. Geotechnical properties and microstructure of clay contaminated with urban wastewater and remediated with α-Aluminum oxide/α-Iron oxide nanohybrid. Soil Sediment Contam. 2023;32:812–42. doi: 10.1080/15320383.2022.2143479.
[3] Baah DS, Foli G, Gikunoo E, Gidigasu SSR. Spatial distribution and potential ecological risk assessment of trace metals in reclaimed mine soils in Abuakwa South Municipal, Ghana. Soil Sediment Contam. 2023;32:692–712. doi: 10.1080/15320383.2022.2128301.
[4] Nasiri M, Hajiazizi M, Jongpradist P, Mazaheri AR. Time-dependent behavior of crude oil-contaminated sands under static and dynamic states. Soil Sediment Contam Int J. 2024;33:353–74. doi: 10.1080/15320383.2023.2204981.
[5] Chen S, Hou X, Luo T, Yu Y, Jin L. Effects of MgO nanoparticles on dynamic shear modulus of loess subjected to freeze-thaw cycles. J Mater Res Technol. 2022;18:5019–31. doi: 10.1016/J.JMRT.2022.05.013.
[6] Xia WY, Du YJ, Li FS, Li CP, Yan XL, Arulrajah A, et al. In-situ solidification/stabilization of heavy metals contaminated site soil using a dry jet mixing method and new hydroxyapatite based binder. J Hazard Mater. 2019;369:353–61. doi: 10.1016/J.JHAZMAT.2019.02.031.
[7] Benaouag N, Sardin M, Arrar J, Bentahar F. Migration of naphthalene through low organic content sandy soil columns: comparison of unsaturated and saturated conditions. Soil Sediment Contam. 2018;27:408–25. doi: 10.1080/15320383.2018.1465889.
[8] Moghal AAB, Lateef MA, Mohammed SAS, Lemboye K, Chittoori BCS, Almajed A. Efficacy of enzymatically ınduced calcium carbonate precipitation in the retention of heavy metal ions. Sustainability. 2020;12:7019. doi: 10.3390/SU12177019.
[9] Husaini A, Roslan HA, Hii KSY, Ang CH. Biodegradation of aliphatic hydrocarbon by indigenous fungi isolated from used motor oil contaminated sites. World J Microbiol Biotechnol. 2008;24:2789–97. doi: 10.1007/S11274-008-9806-3.
[10] Zhou Y, Liu Y. China's fight against soil pollution. Science (80). 2018;362:298. doi: 10.1126/SCIENCE.AAV4061.
[11] Elsaigh WAH, Oluremi JR. Assessment of geotechnical properties of oil contaminated subgrade soil: Review. Soil Sediment Contam Int J. 2022;31:586–610. doi: 10.1080/15320383.2021.1985079.
[12] Ostovar M, Ghiassi R, Mehdizadeh MJ, Shariatmadari N. Effects of crude oil on geotechnical specification of sandy soils. Soil Sediment Contam. 2020;30:58–73. doi: 10.1080/15320383.2020.1792410.
[13] Ma Q, Xiang JC, Yang YC, Xiao HL, Wan J. Study on the mechanical properties of flax fiber-reinforced silty clay contaminated by zinc-ion solution. Environ Technol (United Kingdom). 2021;42:1071–83. doi: 10.1080/09593330.2019.1652697.
[14] Mir B, Amin F, Majid B. Some studies on physical and mechanical behaviour of dredged soil from flood spill channel of Jhelum River, Srinagar. Acta Ing Civ. 2016;1:1–7.
[15] Firoozi AA, Guney Olgun C, Firoozi AA, Baghini MS. Fundamentals of soil stabilization. Int J Geo-Eng. 2017;8:1–16. doi: 10.1186/S40703-017-0064-9.
[16] Ghosh D, Bhattacharyya KG. Adsorption of methylene blue on kaolinite. Appl Clay Sci. 2002;20:295–300. doi: 10.1016/S0169-1317(01)00081-3.
[17] Salimi M, Ghorbani A. Mechanical and compressibility characteristics of a soft clay stabilized by slag-based mixtures and geopolymers. Appl Clay Sci. 2020;184:105390. doi: 10.1016/J.CLAY.2019.105390.
[18] Rasool Haji T, Ahmed Mir B. Effect of nano-gypsum on mechanical properties cement admixed marginal silty soil. Constr Build Mater. 2023;408:133639. doi: 10.1016/J.CONBUILDMAT.2023.133639.
[19] Wani KMNS, Mir BA. A laboratory-scale study on the bio-cementation potential of distinct river sediments ınfused with microbes. Transp Infrastruct Geotechnol. 2021;8:162–85. doi: 10.1007/S40515-020-00131-W/FIGURES/14.
[20] Essienubong I, Okechukwu E, Ejuvwedia S. Effects of waste dumpsites on geotechnical properties of the underlying soils in wet season. Environ Eng Res. 2019;2:289–97. doi: 10.4491/eer.2018.162.
[21] Shimobe S, Spagnoli G. Relationships between strength properties and Atterberg limits of fine-grained soils. Geomech Geoeng. 2022;17:1443–57. doi: 10.1080/17486025.2021.1940317.
[22] Ahmed SM, Agaiby SS. Strength and stiffness characterization of clays using Atterberg limits. Transp Geotech. 2020;25:100420. doi: 10.1016/J.TRGEO.2020.100420.
[23] Chen Z, Ge S, Zhang Z, Du Y, Yao B, Xie H, et al. Soil moisture but not warming dominates nitrous oxide emissions during freeze–thaw cycles in a qinghai–tibetan plateau alpine meadow with discontinuous permafrost. Front Ecol Evol. 2021;9:1–12. doi: 10.3389/fevo.2021.676027.
[24] Wang G, Bian X, Wang YJ, Cui YJ, Zeng LL. Effect of organic matter content on Atterberg limits and undrained shear strength of river sediment. Mar Georesour Geotechnol. 2022;40:1060–72. doi: 10.1080/1064119X.2021.1961955.
[25] Singh SK, Srivastava RK, John S. Studies on soil contamination due to used motor oil and its remediation. Can Geotech J. 2009;46:1077–83. doi: 10.1139/T09-047.
[26] Mir BA, Wani AR, Wani KMNS. Influence of municipal solid waste leachate on the geotechnical properties of soil. Indian Geotech J. 2025;1–20. doi: 10.1007/S40098-025-01175-W.
[27] Izdebska-Mucha D, Trzciński J. Clay soil behaviour due to long-term contamination by liquid petroleum fuels: microstructure and geotechnical properties. Bull Eng Geol Environ. 2021;80:3193–206. doi: 10.1007/S10064-020-02084-3.
[28] Liu ZB, Liu SY, Cai Y. Engineering property test of kaolin clay contaminated by diesel oil. J Cent South Univ. 2015;22:4837–43. doi: 10.1007/S11771-015-3035-3.
[29] Raja K, Venkatachalam S, Vishnuvardhan K, Siva Rama Krishnan R, Tamil Selvan V, Vetriselvan N. A review on soil stabilization using rice husk ash and lime sludge. Mater Today Proc. 2022;65:1205–12. doi: 10.1016/J.MATPR.2022.04.178.
[30] Karami H, Pooni J, Robert D, Costa S, Li J, Setunge S. Use of secondary additives in fly ash based soil stabilization for soft subgrades. Transp Geotech. 2021;29:100585. doi: 10.1016/J.TRGEO.2021.100585.
[31] Reiterman P, Mondschein P, Doušová B, Davidová V, Keppert M. Utilization of concrete slurry waste for soil stabilization. Case Stud Constr Mater. 2022;16:e00900. doi: 10.1016/J.CSCM.2022.E00900.
[32] Harianto T, Utami WD. Effect of mineral additives on the strength characteristics of a laterite soil. Lect Notes Civ Eng. 2021;144 LNCE:423–31. doi: 10.1007/978-981-16-0077-7_37.
[33] Gul N, Mir BA. Influence of glass fiber and cement kiln dust on physicochemical and geomechanical properties of fine-grained soil. Innov Infrastruct Solut. 2022;7:1–15. doi: 10.1007/S41062-022-00943-4.

[34] Wani KMNS, Mir BA. Stabilization of weak dredged soils by employing waste boulder crusher dust: a laboratory study. Geotech Geol Eng. 2020;38:6827–42. doi: 10.1007/S10706-020-01472-6.
[35] Nachtegaal M, Marcus MA, Sonke JE, Vangronsveld J, Livi KJT, van Der Lelie D, et al. Effects of in situ remediation on the speciation and bioavailability of zinc in a smelter contaminated soil. Geochim Cosmochim Acta. 2005;69:4649–64. doi: 10.1016/J.GCA.2005.05.019.
[36] Oprčkal P, Mladenovič A, Zupančič N, Ščančar J, Milačič R, Zalar Serjun V. Remediation of contaminated soil by red mud and paper ash. J Clean Prod. 2020;256:120440. doi: 10.1016/J.JCLEPRO.2020.120440.
[37] Mamindy-Pajany Y, Geret F, Roméo M, Hurel C, Marmier N. Ex situ remediation of contaminated sediments using mineral additives: Assessment of pollutant bioavailability with the Microtox solid phase test. Chemosphere. 2012;86:1112–6. doi: 10.1016/J.CHEMOSPHERE.2011.12.001.
[38] Ali A, Mir BA, Gul N, Malik FZ. Strength and microstructural behavior of soft soil treated with zeolite nanoparticles. Transp Infrastruct Geotechnol. 2023;10:1239–54. doi: 10.1007/S40515-022-00261-3.
[39] Scrivener KL. Nanotechnology and cementitious materials. Nanotechnol Constr. 2009;3:37–42. doi: 10.1007/978-3-642-00980-8_4.
[40] Mir BA, Reddy SH. Mechanical behaviour of nano-material (Al_2O_3) stabilized soft soil. Int J Eng. 2021;34:636–43. doi: 10.5829/IJE.2021.34.03C.07.
[41] Wang Z, Sun J, Wang Y, Guo H, Aryana SA. Optimum concentration of fly ash nanoparticles to stabilize CO_2 foams for aquifer and soil remediation. J Contam Hydrol. 2021;242:103853. doi: 10.1016/J.JCONHYD.2021.103853.
[42] Alazaiza MYD, Albahnasawi A, Ali GAM, Bashir MJK, Copty NK, Amr SSA, et al. Recent advances of nanoremediation technologies for soil and groundwater remediation: A Review. 2021;13:2186. doi: 10.3390/W13162186.
[43] Mir BA, Hariprasad Reddy S. Enhancement in shear strength characteristics of soft soil by using nanomaterials. Lect Notes Civ Eng. 2021;90:421–35. doi: 10.1007/978-3-030-51354-2_39.
[44] Mohammed SAS, Moghal AAB. Efficacy of nano calcium silicate (NCS) treatment on tropical soils in encapsulating heavy metal ions: leaching studies validation. Innov Infrastruct Solut. 2016;1:1–12. doi: 10.1007/S41062-016-0024-9.
[45] Kumari N, Mohan C. Basic of clay minerals and their characteristic properties. In: Nascimento G, editor. Clay and clay minerals. United Kingdom: IntechOpen; 2021. p. 15–45.
[46] General Directorate of Mineral Research and Exploration (GDMRE). Clay deposits map of Turkey. Ankara, Turkey: GDMRE, 2022.
[47] ASTM International. ASTM D854-02, Standard test method for specific gravity of soil solids by water pycnometer. USA: West Conshohocken, PA; 2017.
[48] ASTM International. ASTM D4318-10e1, Standard test methods for liquid limit. Plastic limit. and plasticity index of soils. USA: West Conshohocken, PA; 2017.
[49] ASTM International. ASTM D698-00ae1, Standard test methods for laboratory compaction characteristics of soil using standard effort (12.400 ft-lbf/ft^3 (600 kN-m/m^3)). USA: West Conshohocken, PA; 2017.
[50] Srivastava L, Paramkusam BR, Prasad A. Indian Geotechnical Conference-2010. Stabilisation Engine Oil Contam. Soil Using Cem. Kiln Dust, IGS Mumbai Chapter & IIT Bombay; 2010. p. 389–92.
[51] Zhongjiang H, Shouxi C, Min L, Zhongjiang H, Shouxi C, Min L. Effect of wetting and drying cycles on the compressive strength of oil-contaminated soil treated with lime and fly ash. J Eng Geol. 2018;26:438–44. doi: 10.13544/J.CNKI.JEG.2017-043.
[52] Li M, Ma C, Sun ZM, Yao XY. Mechanical properties distribution of lime-fly ash solidified oil contaminated soil in a coastal environment. Eur J Environ Civ Eng. 2022;26:3027–42. doi: 10.1080/19648189.2020.1781695.
[53] CJM, Shetty SS, Venkat Reddy D, Istijono B. Experimental study on lateritic soil stabilization with waste engine oil and lime. Turk J Comput Math Educ. 2021;12:102–10.
[54] Mir BA, Sridharan A. Physical and compaction behaviour of clay soil-fly ash mixtures. Geotech Geol Eng. 2013;1059–72. doi: 10.1007/s10706-013-9632-8.
[55] ASTM International. ASTM D2166, Standard test method for unconfined compressive strength of cohesive soil. West Conshohocken, PA: ASTM International; 2010.
[56] Jalal FE, Mulk S, Memon SA, Jamhiri B, Naseem A. Strength, hydraulic, and microstructural characteristics of expansive soils ıncorporating marble dust and rice husk ash. Adv Civ Eng. 2021;2021:9918757. doi: 10.1155/2021/9918757.
[57] Zhang Y, Guo S, Yin X, Han SL, Shao S. Evolution of the anti-weathering characteristics of clay at earthen sites treated with K_2SiO_3 solutions: Micromechanism analysis based on SEM tests. Bull Eng Geol Environ. 2022;81:1–13. doi: 10.1007/S10064-022-02926-2/FIGURES/13.
[58] Li L, Zhang J, Xiao H, Hu Z, Wang Z. Experimental investigation of mechanical behaviors of fiber-reinforced fly ash-soil mixture. Adv Mater Sci Eng. 2019;2019:1050536. doi: 10.1155/2019/1050536.
[59] Zabielska-Adamska K. Characteristics of compacted fly ash as a transitional soil. Materials. 2020;13:1387. doi: 10.3390/MA13061387.
[60] Li LH, Yu CD, Xiao HL, Feng WQ, Ma Q, Yin JH. Experimental study on the reinforced fly ash and sand retaining wall under static load. Constr Build Mater. 2020;248:118678. doi: 10.1016/J.CONBUILDMAT.2020.118678.
[61] Ahmed AGA. Fly ash utilization in soil stabilization. Int Conf Civil Biol Environ Eng. 2014. p. 76–8. doi: 10.15242/IICBE.C514601.
[62] Bose B. Geo-Engineering properties of expansive soil stabilized with fly ash. Electron J Geotech Eng. 2012;17:1339–53.
[63] Mir BA. Some studies on the effect of fly ash and lime on physical and mechanical properties of expansive clay. Trans B Geotech Eng. 2015;13(3):203–12.
[64] Nazir AK. Effect of motor oil contamination on geotechnical properties of over consolidated clay. Alex Eng J. 2011;50:331–5. doi: 10.1016/J.AEJ.2011.05.002.
[65] Dindar E, Topaç Şağban FO, Başkaya HS. Variations of soil enzyme activities in petroleum-hydrocarbon contaminated soil. Int Biodeterior Biodegrad. 2015;105:268–75. doi: 10.1016/J.IBIOD.2015.09.011.
[66] Gautam P, Bajagain R, Jeong SW. Combined effects of soil particle size with washing time and soil-to-water ratio on removal of total petroleum hydrocarbon from fuel contaminated soil. Chemosphere. 2020;250:126206. doi: 10.1016/J.CHEMOSPHERE.2020.126206.
[67] Consoli NC, Lopes LdaS, Prietto PDM, Festugato L, Cruz RC. Variables controlling stiffness and strength of lime-stabilized soils. J Geotech Geoenviron Eng. 2011;137:628–32. doi: 10.1061/(ASCE)GT.1943-5606.0000470.
[68] Moghal Baig AA, Sivapullaiah PV. Effect of pozzolanic reactivity on compressibility characteristics of stabilised low lime fly ashes

compressibility of low lime fly ashes. Geotech Geol Eng. 2011;29:665–73. doi: 10.1007/s10706-011-9408-y.

[69] Jahandari S, Mojtahedi SF, Zivari F, Jafari M, Mahmoudi MR, Shokrgozar A, et al. The impact of long-term curing period on the mechanical features of lime-geogrid treated soils. Geomech Geoeng. 2022;17:269–81. doi: 10.1080/17486025.2020.1739753.

[70] Venkata Vydehi K, Moghal AAB. Effect of biopolymer ınclusion and curing conditions on the failure strain and elastic modulus of cohesive soil. Lect Notes Civ Eng. 2023;297:257–64. doi: 10.1007/978-981-19-6727-6_23.

[71] Zhou N, Ouyang S, Cheng Q, Ju F. Experimental study on mechanical behavior of a new backfilling material: Cement-treated marine clay. Adv Mater Sci Eng. 2019;2019:1261694. doi: 10.1155/2019/1261694.

[72] Oluwatuyi OE, Ojuri OO, Khoshghalb A. Cement-lime stabilization of crude oil contaminated kaolin clay. J Rock Mech Geotech Eng. 2020;12:160–7. doi: 10.1016/J.JRMGE.2019.07.010.

[73] Saberian M, Jahandari S, Li J, Zivari F. Effect of curing, capillary action, and groundwater level increment on geotechnical properties of lime concrete: Experimental and prediction studies. J Rock Mech Geotech Eng. 2017;9:638–47. doi: 10.1016/J.JRMGE.2017.01.004.

[74] Singh T, Patnaik A, Chauhan R. Optimization of tribological properties of cement kiln dust-filled brake pad using grey relation analysis. Mater Des. 2016;89:1335–42. doi: 10.1016/J.MATDES.2015.10.045.